

MOHAMED IKRAM BIN MOHAMED KHAIRI

B. ENG. (HONS) MECHANICAL ENGINEERING

JANUARY 2020

COMPUTATIONAL FLUID DYNAMIC (CFD)  
SIMULATION OF SLUG FLOW WITHIN PIPE BEND AND  
PIPE ELBOW WHICH INDUCE VIBRATION

**MOHAMED IKRAM BIN MOHAMED KHAIRI**

MECHANICAL ENGINEERING  
UNIVERSITI TEKNOLOGI PETRONAS

JANUARY 2020

## **CERTIFICATION OF APPROVAL**

### **Computational Fluid Dynamic (CFD) Simulation of Slug Flow Within Pipe Bend and Pipe Elbow Which Induce Vibration**


by

**MOHAMED IKRAM BIN MOHAMED KHAIRI**

22731

A project dissertation submitted to the  
Mechanical Engineering Programme  
Universiti Teknologi PETRONAS  
in partial fulfilment of the requirement for the  
**BACHELOR OF ENGINEERING (Hons)**  
**(MECHANICAL ENGINEERING)**

Approved by,

---

(Dr. William Pao)

**UNIVERSITI TEKNOLOGI PETRONAS**  
**TRONOH, PERAK**  
**JANUARY 2020**

## **CERTIFICATION OF ORIGINALITY**

This is to certify that I am responsible for the work submitted in this project, that the original work is my own except as specified in the references and acknowledgements, and that the original work contained herein have not been undertaken or done by unspecified sources or persons.



---

(MOHAMED IKRAM BIN MOHAMED KHAIRI)

## **ABSTRACT**

Multi-phase flow is any fluid stream consisting of more than one phase or component, for example, gas-liquid stream, liquid-liquid flow, solid fluid stream, or solid-fluid gas stream. It is common in fluid systems, in particular in oil and gas hydrocarbon conveying systems which produce natural gas and crude oil at the same time. A significant response from flux-induced vibration can lead to potential fatigue damage or uncontrolled vibration when the frequency of excitation matches the piping system's natural frequencies, especially in cases where oil produces dense sand particles or slow flows in the flow-lines. This is why it is important to investigate the impact of the oil-gas-water mix on pipeline structure. Due to its difficulty and unpredictability, multi-phase flow problems remain a concern for industry. The present paper analyses the interaction between the fluid-structure fluid and a pipe bend to determine the resultant vibrations generated by the two-phase fluid flux. For research there are two pipe bend models with different bending upstream and downstream lengths. Natural frequencies are eliminated and numerical simulations are performed by the ANSYS Workbench using the CFD solver (ANSYS FLUENT). The frequency of vibrations are obtained and compared with naturally occurring frequencies to assess the correct degree of risk through the transformation of the time domain results into frequency domain.

## ACKNOWLEDGEMENT

My completion of Final Year Project I would not be a triumph without the assistance and direction from my supervisor and colleagues. So, I would like to recognize my heartfelt gratitude to those I honour in realizing the progress of Final Year Project I.

First of all, I would like to extend my sincere thanks to Dr William Pao King Soon, my direct supervisor, for his valuable supervision, encouragement, assistance and assistance during my project. In particular on the technical aspects, I would like to thank him for his work at Universiti Teknologi PETRONAS.

I would also like to thank Dr. Shakif Nasif which had greatly assisted me in learning the ANSYS Software from the beginning. I additionally wish to offer my thanks to my kind colleagues, who were consistently there to give significant recommendations and remarks on my works for further improvement.

Last but not least, I wish to thank my parents and the members of my family for their support. I managed to perform well and persevered through any challenges faced during the project, with their help.

# TABLE OF CONTENTS

CERTIFICATION OF APPROVAL	i
CERTIFICATION OF ORIGINALITY	ii
ABSTRACT	iii
ACKNOWLEDGEMENT	iv
LIST OF FIGURES	vii
LIST OF TABLES	viii
CHAPTER 1: INTRODUCTION	1
1.1 Project Background	1
1.2 Problem Statement	2
1.3 Objectives	3
1.4 Scope of Study	3
CHAPTER 2: LITERATURE REVIEW	4
2.1 Multiphase Flow	4
2.2 Pipe Bend	8
2.3 Flow Pattern of Two Phases Flow	12
CHAPTER 3: METHODOLOGY	17
3.1 Description of the Problem	17
3.2 Multiphase Flow Modeling	19
3.3 Development of Fluid Domain Model	22
3.4 Meshing of Pipe and Fluid Domain	24
3.5 Modal Analysis	25
3.6 Screening Methodology	25
3.7 Project Process Flow Chart	27

3.8 Project Gantt Chart	28
CHAPTER 4: RESULTS AND DISCUSSION	29
4.1 Validation of flow pattern on Baker's map	29
4.2 The transition of slug flow pattern in a horizontal pipe	30
4.3 Validation of model against Experimental figures	32
4.4 Parametric analysis on diameter ratio of the orifice plate	35
CHAPTER 5: CONCLUSIONS AND RECOMMENDATIONS	46
REFERENCES	48

## LIST OF FIGURES

Figure 1.2.1: Dislodging of supporting mechanisms in pipeline [3].	2
Figure 2.1.1: Flow Regimes in Horizontal Pipes (Source: <a href="https://build.openmodelica.org">https://build.openmodelica.org</a> ).	5
Figure 2.1.2 : Flow Pattern Map of Crude Oil and Natural Gas at 68 atm	6
Figure 2.1.3: Gas-Liquid flow Regime Map for Horizontal Pipe. (Adapted from Shell DEP 31.22.05.11):	7
Figure 2.2.1: Summary of the studies in two phase flow and multiphase flow in different types of pipe bend.	8
Figure 2.2.2: Streamlines of the secondary flow in the longitudinal section and the cross section of a 90° bend.	9
Figure 2.3.1: Region of flow components in pipe [6].	13
Figure 2.3.2: Baker Chart [6].	16
Figure 3.1.1: Horizontal bending pipe geometry of the computational modelling.	18
Figure 3.4.1: Mesh Of (A) Pipe Bend (B) Fluid Domain	24
Figure 3.6.1: Locations monitored (At bend)	25
Figure 3.7.1: Project Flow Chart	27
Figure 4.1.1: Contour of water volume fraction on slug development. (a) De Schepper et al. (2008) model, (b) Present model, (c) Mohammed (2016) model.	29
Figure 4.2.1: Water volume fraction contours of slug flow in the pipe.	31
Figure 4.2.2: Time evolution contours of Slug flow and the water volume fraction air-water towards the pipe's elbow for ( $U_{sa} = 3.07$ m/s and $U_{sw} = 0.4$ m/s).	32
Figure 4.3.1: The schematic diagram of the experimental apparatus [16].	33
Figure 4.3.2: The evaluation of slug progression between experimental work and CFD data simulation on water volume fraction for $U_{sa} = 1.88$ m/s, $U_{sw} = 0.77$ m/s (a) Stratified pattern, (b) Crest jump and (c) slug pattern.	34
Figure 4.3.3: Contour of Slug flow water volume fraction, snapshot of experimental works and simulation for $U_{sa} = 1.88$ m/s, $U_{sw} = 0.77$ m/s.	35
Figure 4.4.1: Time record of water volume fraction on the cross sectional pipe located before elbow when increases air superficial velocity from 3.08 m/s to 6.45 m/s with constant water superficial velocity, $U_{sw} = 0.4$ m/s.	37
Figure 4.4.2: The total exerted pressure on elbow's wall against air inlet superficial velocity with r/D ratio from 1.0 to 3.0 for graph (a) (b) (c) (d) with constant inlet $U_{sw}$	



= 0.4 m/s.....	40
Figure 4.4.3: The total exerted pressure on elbow's wall against r/D ratio with air inlet superficial velocity from 3.07 m/s to 6.45 m/s for graph (a) (b) (c) (d) with constant inlet $U_{sw} = 0.4$ m/s.....	42
Figure 4.4.4: The resultant force on elbow's wall against r/D ratio with air inlet superficial velocity from 3.08 m/s to 6.45 m/s for graph (a) (b) (c) (d) with constant inlet $U_{sw} = 0.4$ m/s.....	45

## LIST OF TABLES

Table 2.1.1: Table Comparison of Single Phase and Multiphase.....	4
Table 2.1.2: Flow regimes of a Two-Phase Gas-Liquid Flow .....	5
Table 2.2.1: Critical Analysis.....	10
Table 3.1.1: Properties of Materials used in simulation .....	18
Table 3.3.1: Pipeline parameters. ....	23
Table 3.3.2: Boundary Conditions.....	23
Table 3.4.1: Difference in Mesh properties of FEA and CFD .....	24
Table 3.6.1: Properties measured at locations of interest.....	26
Table 3.8.1: Project Gantt Chart.....	28
Table 4.1.1: Simulation of the air-water operating condition for slug development. .	29
Table 4.4.1: The inlet boundary condition for parametric study.....	36
Table 4.4.2: Approximate time for Slug to arrive at pipe's elbow.....	37
Table 4.4.3: Water volume fraction contour on slug development for each condition of air inlet superficial velocity.....	38
Table 4.4.4: Pressure Contour at Measurement Section 1 and 2 with varies value of r/D ratio and air superficial velocity at constant inlet $U_{sw} = 0.4$ m/s.....	43

# CHAPTER 1:

## INTRODUCTION

### 1.1 Project Background

For the exchange of fluids between two or more remote stations, pipelines are used. In oil and gas processing and distribution plants, gas and liquid two-phase flows in pipelines occurred. Due to the constant supplied energy needs, the transmission pipelines are the main arteries for the petroleum and gas industry.

The simultaneous 2 or more phases through a pipe is called multi-phase flow. The two-phase mix may be carbon / gas (oil & water) and non-solid (carbon & slot) and gas-liquid or gas-pulverized fuel. This can be gas resistant. (pulverized coal) Gas-fluid flow is the most common two-phase flow and can be used in a wide variety of industrial applications in the oil and gas industries, including the chemical industry. In certain cases, a multiphase flow for the oil and natural gas reserves include the upstream piping network and extracting hydrocarbons, such as the spreading of the split pipe, exporting medium and the extraction of oil pumps. For several decades two-stage gas-liquid flows, particularly in the oil and natural gas fields, have been the subject of research interest, operating in several pipelines under various flow conditions.

The pipe flow would have different flow rates depending on the surface gas and fluid velocities respectively. This flow regime will vary from the gentle, smooth layered flow to the rough, scattered ring flow. The slug flow behavior in the pipelines can be attributed to different Fluid properties, including viscosities and densities but particularly surface speeds in both phases. The flow mechanism also puts great importance on the fluid layout of the ducts, including pipe length, diameter, orientation and tilting towards or toward gravity.

## 1.2 Problem Statement

FSI is one of the important keys to flow assurance issues because excessive vibrations arising from FSI can cause dislodging of pipelines from the supporting mechanisms such as hangers and thrust blocks as well as an increased risk for pipe breakage. Whereas, perturbations in velocity and pressure of the flow could cause unsmooth flow and pose great problems to flow assurance as shown in Figure 1.2.1. This problem is magnified in a multiphase flow, especially in a slug flow. To predict the resulting effects of multiphase flow FSI, the first thing needed is to model and predict the detailed behaviour of the multiphase flow as well as the patterns that they exhibit. Then, the piping structure comes into play. In this project, it is within a pipe bend. Turning elements such as T-junctions and bends are the locations that are most subjected to flow-induced forces due to the changes of momentum of the fluids. The effects of fluid flow on the adjacent structure or body, i.e. piping structure, vary with the fluid flow characteristics, including its compositions, density, viscosity, volatility and turbulence.

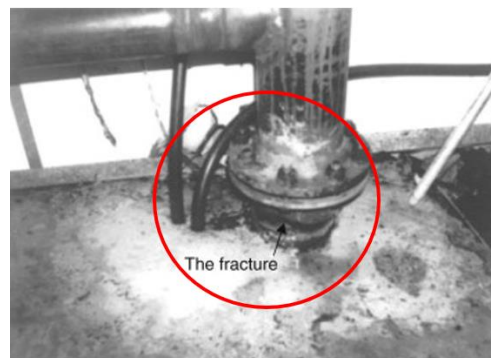


Figure 1.2.1: Dislodging of supporting mechanisms in pipeline [3].

Multiphase flow often presents a far more complex and unpredictable flow behaviour than single phase flow. Consequently, the FSI arising from multiphase flow is difficult to predict. One of the reasons is because the density and other properties of the fluid are very difficult to estimate as different phase and components exist. Simulation often requires very high computing power, not to mention multiphase flow FSI simulation where the model can be very complex. Fortunately, computational methods have evolved over the past decades witnessing the birth of high-performance

computers and powerful computing software such as ANSYS. These breakthroughs have given new breath to FSI modelling and prediction.

However so, even in simplified simulation where only two-phase - crude oil (liquid) and gas phase, the density, compositions, and other properties of the fluid vary from each reservoir depending on its nature, temperature and pressure, age of reservoir and composition. Thus, there are many variables that have to be taken into consideration and there are variables that have to be assumed during multiphase flow FSI simulation.

### 1.3 Objectives

For this project, numerical simulation of liquid-liquid flow is conducted and aimed:

- a) To determine the effect of bending radius on pressure exerted on the wall of elbow that results in flow-induced vibration arising from multiphase flow within a horizontal pipe bend by using Computational Fluid Dynamic (CFD).
- b) To correlate  $r/D$  ratio of pipe's elbow with  $90^\circ$  of bending angle.

### 1.4 Scope of Study

The study's main focus is to construct a two-phase flow simulation in a horizontal pipe with various geometric parameters using ANSYS FLUENT. The Fluid Volume (VOF) model was used to model the slug flow pattern hydrodynamics. The chosen pipe type was circular cross-sectional shapes with an internal diameter of 0.08 m and 12 m long. Isothermal conditions are likely to extend to the internal pipe wall. Air and water served as fluids for operations. The measurement of geometric parameters was bending radius over diameter ( $r / D$ ) ratio while the operating parameter was inlet air and superficial velocity of the water.

## CHAPTER 2:

### LITERATURE REVIEW

#### 2.1 Multiphase Flow

De Schepper et al. (2008) characterizes multiphase flow as a concurrent flow of materials with particular states or stages, for example, gas, fluid or solid. It can likewise be a flow of materials in a similar state or phase however with various compound properties, for example, oil-droplets in water. According to Bakker (2005) also, there are several regimes of multiphase flow. An example distinguishing single phase and multiphase is shown in Table 2.1.1. In the context of this thesis, the main concern is on two-phase gas-liquid flow.

Multiphase flow modelling is a very complex work. Not only there are limitations in time, computing power is also a key to whether or not a multiphase flow can be modelled accurately. Some models have been developed that are suitable for different multiphase flow applications and exhibit different levels of accuracy and applications; they are Eulerian-Lagrangian, Eulerian-Eulerian, Volume of Fluid, etc.

Table 2.1.1: Table Comparison of Single Phase and Multiphase

	Single component	Multi-component
Single Phase	Water Pure Nitrogen	Air H <sub>2</sub> O + Oil Emulsions
Multiphase	Steam bubble in H <sub>2</sub> O Ice Slurry	Coal Particles in Air Sand Particles in H <sub>2</sub> O

Similar to single-phase flow, a multiphase flow follows the three main conservation principles, namely the conservation of mass, momentum and energy. These principles apply for each phase in a multiphase flow. Therefore, there would be

at least two sets of each of the conservation laws in multiphase flow. Simplifications were made by some pioneers such as Kim and Chang (2008) for multiphase flow.

There are several two-phase gas-liquid flow regimes. They are shown in Figure 2.1.1, and are summarized in Table 2.1.2. A flow regime explains how the phases are distributed geometrically. Even influencing phase distribution, velocity distribution and so on is the system in which the fluid flows (Chica, 2012).

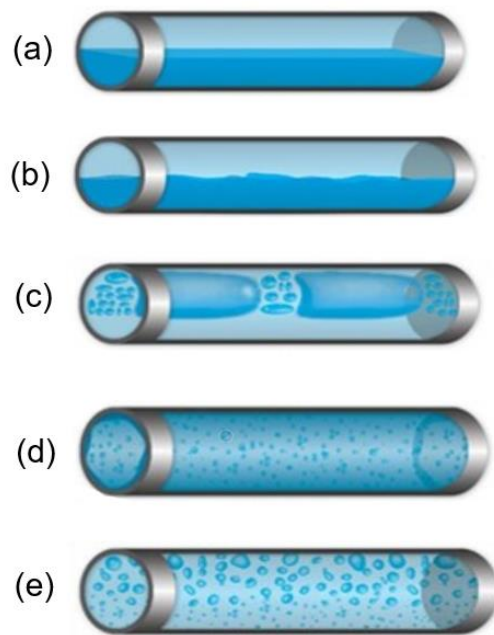


Figure 2.1.1: Flow Regimes in Horizontal Pipes (Source: <https://build.openmodelica.org>)

Table 2.1.2: Flow regimes of a Two-Phase Gas-Liquid Flow

Multiphase Flow Regime	Characteristics
Bubbly flow (a)	Discrete gaseous bubbles in a continuous liquid.
Stratified and free-surface flow (b)	Immiscible fluids isolated by a characterized interface.
Wavy flow (c)	Superficial velocity of gas increases and waves starts forming at the interface boundary due to surface tension.

Slug flow (d)	Discontinuous elongated bubbles separated by chunks of liquids that blocks the pipe.
Annular flow (e)	Continuous liquid around walls, core gas. It occurs because of the high superficial gas velocity as opposed to the air.

As to simulate the flow in the desired flow pattern, a flow regime map is to be referred, such as the Taitel-Dukler flow regime map as shown in Figure 2.1.2. The Taitel-Dukler flow regime map is based on the superficial velocities of the phases. Another flow-regime map as adapted by Shell Design and Engineering Practice (DEP) Standard 31.22.05.11 is the gas-liquid two-phase flow regime map (Figure 2.1.3) based on the Froude numbers of each phase.

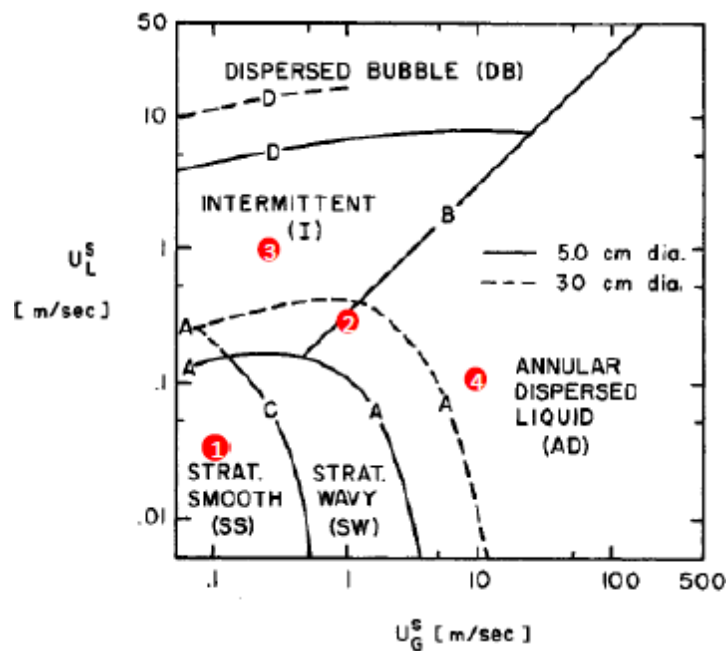


Figure 2.1.2 : Flow Pattern Map of Crude Oil and Natural Gas at 68 atm

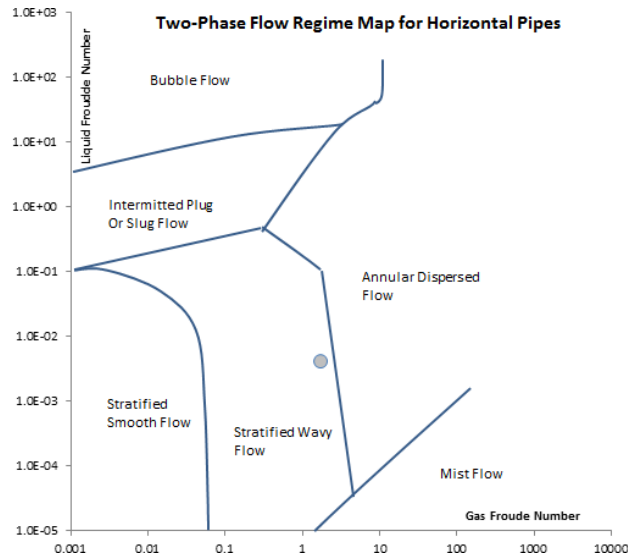


Figure 2.1.3: Gas-Liquid flow Regime Map for Horizontal Pipe. (Adapted from Shell DEP 31.22.05.11):

Chica (2012) developed a screening methodology for assessing flow-induced vibration (FIV) due to multiphase flows using a combination of STAR-CCM+ tool and FEA code ABAQUS. Comparisons were made between two-phase and three-phase flows. Kadri et al. (2012) researched on the suitable parameterization to simulate slug flows using Volume-of-Fluid method. Suitable parameterization is important for accuracy and computation speed. Less compressive schemes are preferred instead of the most compressive scheme because it allows for coarser meshes while maintaining fine accuracy and avoiding numerical errors. Riverin et al. (2006) discussed that the source of FSI excitation can be due to swift changes in flow and pressure or due to mechanical action of the piping. Riverin et al. (2007) successfully simulated two-phase slug flow using ANSYS CFX and validated his results with experiment. The results shown that CFX calculation were very accurate in predicting flow pattern formed by two-phase flow.

De Schepper et al. (2008) argues that unlike single-phase flow where an entrance length of 30 to 50 diameters is required for fully developed turbulent flow, multiphase flow is complex and the corresponding entrance lengths are less well established. He emphasizes that a flow regime map does not always accurately predict a certain flow pattern for a given fluids with given flow rates.



## 2.2 Pipe Bend

The design of pipeline systems needs to go through a series of phases, according to Miwa (2015), which are: initial design, feasibility tests, practical design, optimization and risk assessment. Fast changes in the flow rates and direction of liquid or two-phase piping systems may cause transient pressure producing bursts of pressure and transient forces inside the piping system. Regularly difficult to measure and calculate are the magnitudes of these pressure bursts and force transients. In designing pipe bends, there are a certain standard that have to be followed, especially for the multi- billion-dollar oil and gas application. Figure 2.2.1 shows the summary of the studies in two phase flow and multiphase flow in different types of pipe bend.

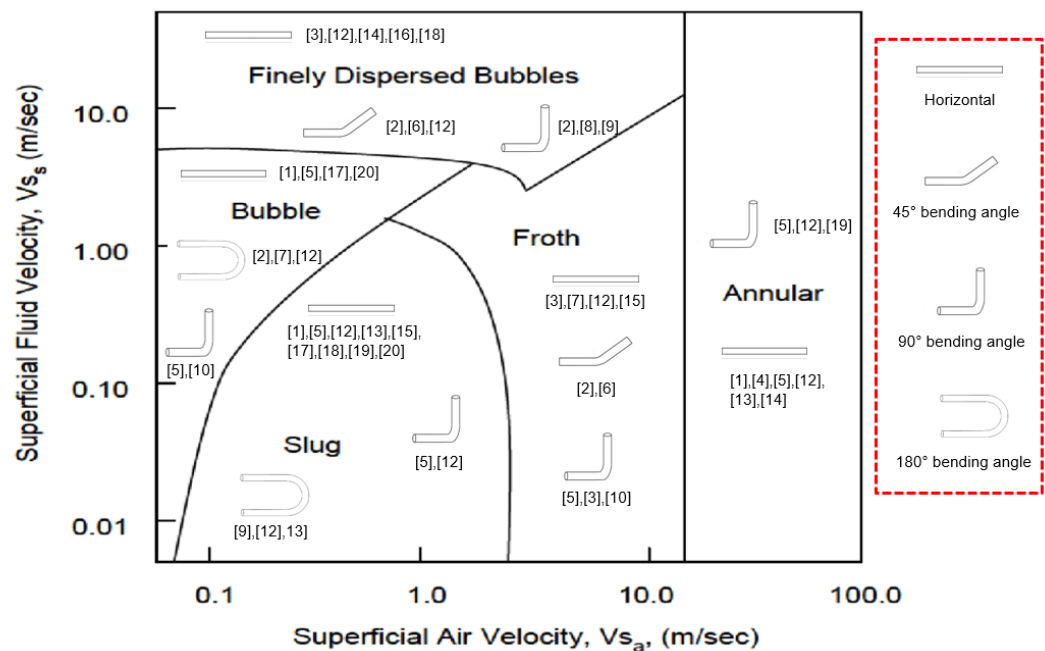


Figure 2.2.1: Summary of the studies in two phase flow and multiphase flow in different types of pipe bend

According to Mazumder (2012) the curvature of the tubular bend produces a centrifugal force which is guided from the momentary core to the outer wall. The combination of the wall boundary layer causes indirect flow by fluid adhesion to the wall and the centrifugal force, as seen in Figure 2.2.2. This secondary stream is optimally compensated by the tube axis. As a consequence, the helical shape becomes simplified by the bending.

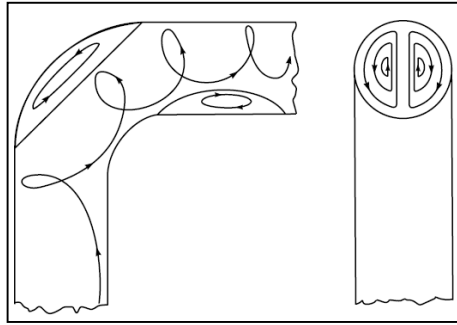
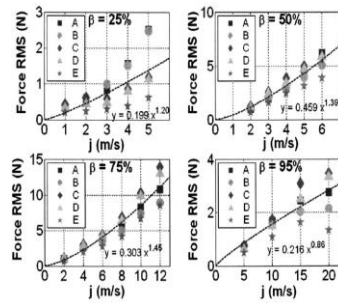


Figure 2.2.2: Streamlines of the secondary flow in the longitudinal section and the cross section of a 90° bend.

In a study conducted by Mazumder, (2012), it was found that in a two- phase bend, the pressure drop is dependent on the  $r/D$  ratio but is independent of pipe diameters. Besides  $r/D$  ratio, the equivalent length to diameter ratio,  $L_e/D$  is also of importance. Mazumder (2012) states that, for a fully-developed flow, a  $L_e/D$  ratio of 100 to 150 is required. Whereas for  $r/D$  ratio, the standard values for a 90° pipe bend are  $4D$  and  $5D$  for bends and  $1.5D$  for elbow according to PETRONAS Technical Standards 31.38.01.11. In an experimental study conducted by Hou et al. in 2014 on the drop in pressure of turbulent through a 90 ° elbow, it was found that axial symmetry features were more compatible with a fluid than fully formed pipe flows, and natural stress distribution of turbulent flows. The bend curvature also intensified the decay in a pipe flow. This was also concluded. A critical analysis is provided in table 2.2.1, which was carried out by studying two-phase flow and multiphase flow in pipe bends.

Table 2.2.1: Critical Analysis

Author / Date	Phase	Geometrical Parameter / Operating Conditions	Remark	Result
Yadav, Worosz, Kim, Tien & Bajorek (2014) [5]	Two-phase flow.	90° vertical-upward elbow. (L/D=3, L/D=9, L/D=21, L/D=33).	<ol style="list-style-type: none"> <li>1. Experiments were carried out on 90° vertical-upward air–water flows.</li> <li>2. The investigation focuses on the effect of the elbow’s length and diameter (L/D) ratio on the dissipation of bubbles across the pipeline system.</li> </ol>	<ol style="list-style-type: none"> <li>1. In single-phase flow conditions the elbow-effects are closely associated with the elbow-effects.</li> <li>2. The elbow effects on the two-phase flow parameters (vibration-inducing bubbles) vanish with an enhanced L / D ratio for the elbow.</li> </ol>
Mazumder (2012) [8]	Multiphase	90° vertical to horizontal elbows. (1.5<r/D>3)	<ol style="list-style-type: none"> <li>1. Experiments were carried out on 90° vertical to horizontal elbows.</li> <li>2. This investigation focuses on the effect of elbow’s bending radius and diameter ratios toward the radial velocity and pressure in the elbow.</li> </ol>	<ol style="list-style-type: none"> <li>1. Variations of r/D ratio resulting in different flow velocities and pressure as increasing r/D ratio effect in the decreasing of flow velocity and pressure in the elbow.</li> <li>2. The pressure across the elbow decreases when the bending radius of the elbow increased.</li> </ol>

<p>Liu, Miwa, Hibiki, Ishii, Morita &amp; Kondoh (2012) [10]</p>	<p>Two-phase flow.</p>	<p>90° horizontal elbow. (Bend radius = 76.2 mm, Pipe Internal Diameter= 52.5 mm) / (U = 0.15 – 4.00 m/s).</p>	<p>1. CFD simulation were carried out on 90° horizontal air–water flows. 2. The investigation focuses on the effect of Superficial Liquid Velocities towards the Force Fluctuation on the elbow of designed pipeline.</p>	<p>1. Force Fluctuation increases as liquid superficial velocity (U) increased. 2. Value of excitation force drastically affects the value of Momentum flux which induce vibration in the pipeline.</p>
<p>Riverin &amp; Pettigrew (2007) [12]</p>	<p>Two-phase flow</p>	<p>1. U-shaped piping. (r/D = 0.5, 2, 5, 7.2m) 2. Void fraction / Volumetric quality (<math>\beta</math>) : 25%, 50%, 75% and 95%.</p>	<p>1. The investigation focuses on the effect of Void fraction towards the Force RMS in the elbow of designed pipeline.</p>	 <p><b>Figure 9:</b> Rms</p>

## 2.3 Flow Pattern of Two Phases Flow

### 2.3.1 Horizontal Flow Schemes in Pipe

The two-phase flux patterns in horizontal pipes are close to vertical flow, but the liquid distribution is determined by gravity. When gravity perpendicular to the pipe axes, the liquid is compressed to the bottom of the tube and to the surface. De Schepper et al. (2008) set out various horizontal pipe flux patterns in gas or liquid flow which are roughly the following categories.:

**Stratified flow:** Two phases are completely segregated at low superficial velocities of liquid and gas. The gas flow is isolated by smooth horizontal interface on top of the oil. However, an increase in gas speed leads to the development of waves on the interface which produce wavy layers.

**Intermittent flow:** For further changes in gas level, interfacial wave rises and a fluid system is known as intermittent flow. This form of flow is a slug and connecting combination. The following are listed in these subcategories:

**Plug flow:** Liquid connections are isolated into this flow network by elongated gas bubbles. On the layer of big waves are the huge bubbles that float along the top of the vessel. Plug flow is often referred to as extended bubble flow.

**Slug flow:** Fluid bubbling aeration happens at high gas levels, producing tiny gas bubbles. The gas bubbles rise and the bubbles stop. The waves of great amplitude can also be seen in the liquid slugs that distinguish these long bubbles. Such waves touch the top of the pipe and produce a flowing slug that flows quickly through the pipe. The two key causes of pipeline fatigue in the flow structure are plug and slug flow.

**Bubbly flow:** The gas bubbles in the upper part of the pipe are completely scattered with a large number of bulbs due to the thriving powers. The turbulence intensity is enough to evenly distribute the bubbles through the pipe at a high fluid level, or if the cuts dominate. The upper component of the pipe pool in bubbles tends to be tidal.

**Annular flow:** As the speed of the gas increases, the liquid forms a ring-film around the tube, which is thicker on the bottom than on the top due to the gravity.

### 2.3.2 Superficial Velocity

In single-phase flow, instantaneous average velocity was also described as volumetric  $Q$  [ $\text{m}^3/\text{s}$ ] divided between cross-sectional pipe area  $A$  [ $\text{m}^2$ ].

The concept of average speed in multi-phase flow is becoming a difficult issue. The region of a certain process, as shown in Figure 2.3.1, varies in time and space and thus the flow no further equals the speed. A network of flows is defined by a superficial speed. Using superficial speed has the advantage of being maintained irrespective of the complexity of the flow mechanism (for incompressible flux without any change of phase), e.g. The superficial speed remains constant even though the speed at the local level is different when the flow rate is moved from the bubble to the slow flow. Maps with the surface gas speed on one axis and the superficial fluid speed on the other are called nutrient diagrams and are used to describe the limits of the various regimes. ANSYS CFD-Post allows users automatically to show superficial rapid velocity or (true) speed variables while viewing the effects of multi-phase simulations.

Sometimes the use of a superficial speed is frequently seen in correlations of pressure drop for porous areas, whether the real porosity or the pore represents flow obstructions. An experimentalist can define his device with superficial or real pace, but it is useful to understand that using superficial velocity is more common when testing data, since this can be measured outside the porous region.

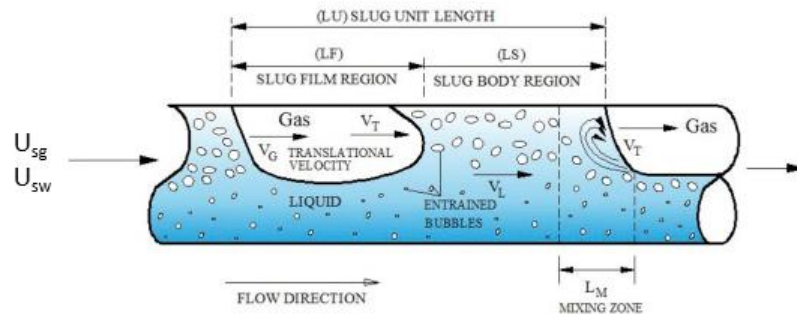


Figure 2.3.1: Region of flow components in pipe [6].

True (phase) velocities are defined as:

$$U_L = \frac{Q_L}{A_L} \quad (2.1)$$

$$U_G = \frac{Q_G}{A_G} \quad (2.2)$$

$U_L$  is superficial velocity of liquid,  $U_G$  is superficial velocity of gas,  $A_L$  is the symbol of area of liquid in the pipe while  $A_G$  is the area of gas concentration in the pipe,  $Q_L$  is liquid volumetric flow rate,  $Q_G$  is gas volumetric flow rate.

The superficial gas and liquid velocities and mixture velocity are defined by:

$$U_{SL} = \alpha_L U_L = \frac{Q_L}{A} \quad (2.3)$$

$$U_{SG} = \alpha_G U_G = \frac{Q_G}{A} \quad (2.4)$$

$$\alpha_G = \frac{A_G}{A} \quad (2.5)$$

$$\alpha_L = \frac{A_L}{A} \quad (2.6)$$

$$\alpha_G + \alpha_L = 1 \quad (2.7)$$

$$U_M = U_{SL} + U_{SG} \quad (2.8)$$

Where  $U_{SL}$  is a superficial liquid speed,  $U_{SG}$  is a superficial gas speed,  $\alpha_G$  (measured fraction) and  $\alpha_L$  (liquid holdup), respectively, the volume fraction of gas and liquid,  $A$  is a sectional region, and  $U_M$  has a mixed speed.

The total speed is proportionate to that of the volumetric flow that can be observed, as the average instantaneous velocity of the loop would have been by taking the entire cross-section of the pipe. Since it takes just half, surface speed tends to be less than the real average speed.

### 2.3.3 Categories of Flow Regime Map in Pipe

The flow pattern map of Baker (1954) is one of the oldest and perhaps most frequently employed, particularly in the petroleum sector. Based on industry-relevant data, the map was created by visually evaluating the different flow regimes. They researched transformational terms between the five flow regimes of stratified,

stratified, sluggish, ring, and bubbly flow, beginning at each stage of laminated flow with a one-dimensional energy balance. He addressed this issue with the visualization of a layered fluid and then understood how to anticipate the change from the layered flux and how this process can be accomplished. The layered flow doesn't have to happen because the way they form in a certain flow pattern is established in a certain gas and liquid flow rate. Slow flows may also be referred to as this method. Taitel and Dukler created a mechanical flow model diagram, which can predict a two-phase flow pattern under various system conditions.

### 2.3.3.1 Two Phase Baker Map

For many industrial applications, the two-stage gas-liquid flows through the horizontal pipeline. The key prevision in the field of multiphased flow insurance is a two-phase gas-liquid flow supply in the pipeline. Typically, defined flow pattern maps are used to define flow pattern type, without complete calculation. The map is created by classifying different flow schemes on the basis of data from industry. In the measurements of flow-parameters on pipes (pressure-dependent, void-factor, heat and mass transfer etc.) Baker (1954) [6] first commented on the importance of flow patterns. During his work, he introduced in a circular pipe, as seen in Figure 2.3.2, the first flow design plan for the horizontal flow. He has also identified fluid patterns in plug stream, wave flow, bubble flow, ring flow, stratified flow and close flows. His experimental data are well matched with the widespread flow diagram.

$G_L/G_G$  are shown in figure 2.3.2, which varies from the flow pattern characteristics that suit Baker's chart according to its boundaries by the role of the mass flows of gas,  $G_G$  and liquid and gas mass flow ratio.

Parameters for the map to be represented in any gas / liquid mixture other than the normal flow mix are  $\lambda$  and  $\psi$  dimensional parameters. In the rising mixture at atmosphere and room temperatures of 25 ° C air and water would possibly equivalently have the  $\lambda$  and  $\psi$  parameters. The correct value of  $\lambda$  and  $\psi$  is determined by modeling the two-stakes dynamics of any gaseous ( $G_G$ ) and liquid ( $G_L$ ) at various temperature and pressure levels using the same



diagram. Although solid lines illustrate transition flow systems for region-to-area as shown in Figure 2.3.2, they actually represent large transition regions.

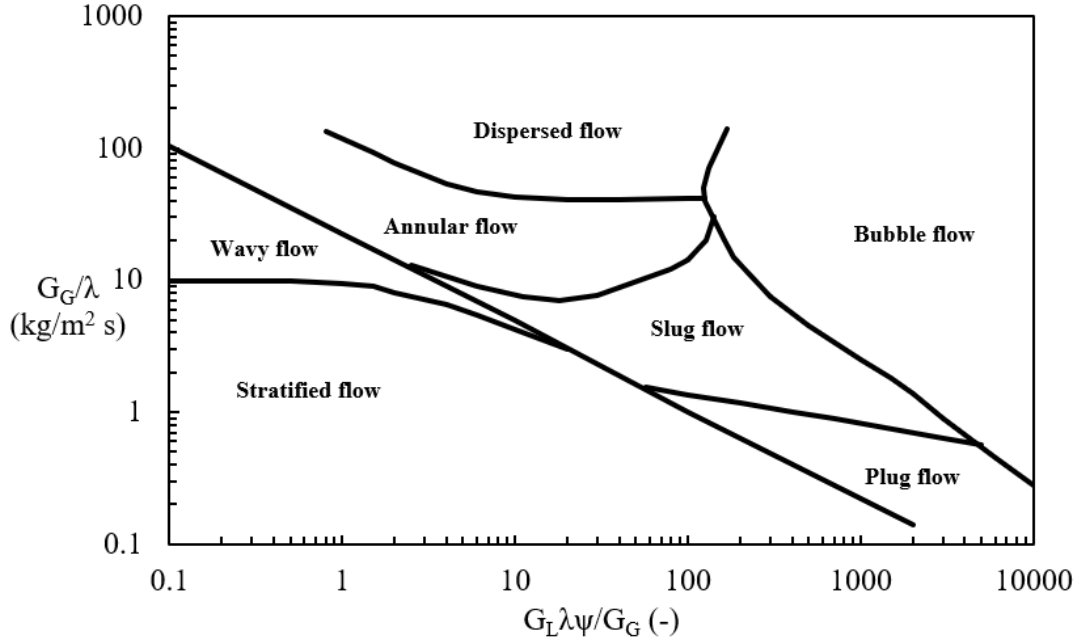


Figure 2.3.2: Baker Chart [6].

For use of the map, fluid and gas flux (air, vapor) must be assessed first. The  $\lambda$  and  $\psi$  parameters of Baker are then determined. The parameter of the gas phase is  $\lambda$  and the fluid phase is  $\psi$ . The x-axis and y-axis values are then determined to evaluate the flow system concerned. Those dimensional parameters of the gas and liquid phase mass flux are given by:

$$\lambda = \left[ \left( \frac{\rho_G}{\rho_a} \right) \left( \frac{\rho_L}{\rho_w} \right) \right]^{-0.5} \quad (2.9)$$

$$\psi = \frac{\sigma_w}{\sigma} \left[ \left( \frac{\mu_L}{\mu_w} \right) \left( \frac{\rho_w}{\rho_L} \right)^2 \right]^{1/3} \quad (2.10)$$

Where  $\lambda$  and  $\psi$  are dimensionless parameters that were used in the governing equations, where  $\rho_G$ ,  $\rho_L$ ,  $\rho_a$  and  $\rho_w$  are respectively the density of gas, liquid, air and water.  $\mu_L$  and  $\mu_w$  are viscosity of liquid and water, respectively,  $\sigma_w$  is surface tension of water and  $\sigma$  is the symbol of gas-liquid surface tension.

## CHAPTER 3:

### **METHODOLOGY**

Throughout the project, comprehensive preliminary studies into previous researches have been carried out. This study is started with the development of a pipe bend. As discussed in Chapter 2, pipe bends require certain standards and requirements, and the model used is in comply with it to validate for the practical cases. Based on the corresponding scope of study, numerical simulation is set up and performed on the pipe bend model to generate the outcomes. The results are then validated with experimental data, and afterward being analysed to study the two-phase separation efficiency to meet the pre-stated objectives.

The numerical technique of Computational fluid dynamic (CFD) will be used to be model and the proposed methodology is as presented. For the behaviour of multiphase flow in pipe bend, the results will be simulated by using ANSYS FLUENT.

#### **3.1 Description of the Problem**

In this analysis, the two-phase horizontal flow schemes and slug flow generation were simulated by solving the governing equations in the commercial FLUENT 16.1.

##### **3.1.1 Geometry**

For the case studies modelled, the general structure of horizontal bending pipe flow is shown in Figure 3.1.1. This consists of a 0.08m (3.15”) internal pipe of 8 m in length. The diameter of the pipe is aligned with the x axis and is located around different measuring sections of the horizontal pipes.

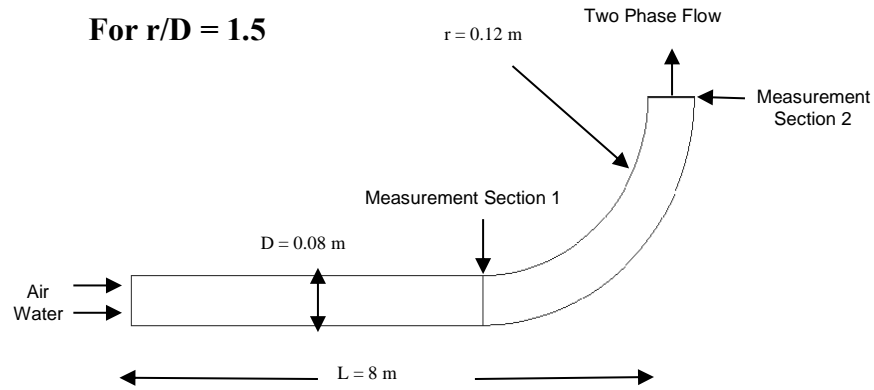


Figure 3.1.1: Horizontal bending pipe geometry of the computational modelling.

### 3.1.2 Flow Specification

As is done in Baker's experimental works (De Schepper et al., 2008), the two-phase air-water flows was channeled at the inlet portion of the pipe's numerical flow domain and are eventually discharged at atmospheric pressure through the outlet. The flow conditions to form or to generate the slug-flow transition are defined in Chapter 4.

### 3.1.3 Fluid Properties

The properties of the fluids (air and water) used in the simulation are as given in Table 3.1.1.

Table 3.1.1: Properties of Materials used in simulation

Fluid	Density ( $\text{kg/m}^3$ )	Viscosity (Pa s)	Surface tension (N/m)
Air	1.225	0.000018	0.0719404
Water-liquid	998.2	0.001003	
Gas vapor	17.1	0.0000115	0.018653
Oil	810.3	0.004652	

## 3.2 Multiphase Flow Modeling

The multi-phase flow processing shows different flow schemes from one to the other, depending on the operating conditions. When modeling the multiphase flow, three main steps need to be addressed. The first step in the process of model selection is to determine how many phases and how often they are flowing. Secondly, the formulation of controlled equations plays a significant role in building a multi-phase flow model. The local, immediate mass mass, impulse and energy conservation equations are formulated into the control volume by all flow problems and any flow actions to transfer all phases of the numerical simulation.

FLUENT 16.1 approach for discrete governing equations is based on the Finite Volume Method (FVM) approach (Vallee, 2007). The present paper employs the Euler Multiphase VOF process in the two separate stages of liquid and gas. The k- $\epsilon$  model was used to treat fluid turbulence events and was described in Section 3.2.3.

### 3.2.1 Volume of Fluid Model (VOF)

Computational Fluid Dynamics (CFD) is one of the most common multi-stage flow modeling methods or techniques. The VOF model is the only way to track and document properly the interface between the two phases. The movements of the interface are followed by itself in this process; instead, every phase volume changes time in each cell and the interface of the two phases in the new periods is reconstructed from the volume values of a new time. This trend is explained by the fact that VOF models are sometimes referred to as volume control methods (Mazumder, 2012).

The VOF model maps and captures the interaction between the gas and fluids interaction, finds a solution for the collection of single impulses and controls the amount of gas and liquids in the area (De Schepper 2008). (Friedrich-, 2008). If the fluid flow in a horizontal conduit and a gas sheet are put on top of the fluid, a separate gas inlet may be identified in a border state via a VOF approach. Number fractions of all phases are uniformly specified in every number of numerical controls. All variables and features are exchanged through the stages and connected with the local volume section. Therefore, all variables and features are average volume values, depending on the volume fraction, in any particular computational cell, and they are representative either of one stage or of the process combination.

Consequently, variables are assigned to each computational unit based on these appropriate properties of  $\alpha_k$ . The density ( $\rho$ ) and viscosity ( $\mu$ ) of gas-liquid transmission may be measured as:

$$\rho = \alpha_L \rho_L + \alpha_G \rho_G \quad (3.1)$$

$$\mu = \alpha_L \mu_L + \alpha_G \mu_G \quad (3.2)$$

### 3.2.2 Governing Equations

The governing equations for Eulerian multiphase model can be summarized as follows in Eqn. 3.3, Eqn. 3.4 and Eqn. 3.5.

#### 3.2.2.1 Conservation of Mass

$$\frac{\delta(\alpha_k \rho_k)}{\delta t} + \frac{\delta}{\delta x} (\alpha_k \rho_k v_k) = \Gamma_{ki} + \Gamma_{kw} \quad (3.3)$$

The first, second, third and fourth term of the equation refers to the accumulated mass inside the pipe, total mass flow into the pipe, the mass flow from other phases and total mass flow from other external sources respectively.

#### 3.2.2.2 Conservation of Momentum

$$\sum_{k=1}^N R_{ki} + S_{ki} + v_k \Gamma_{ki} = 0 \quad (3.4)$$

In addition to the Newton's second law, additional forces are considered to account for the phase-to-phase interactions. These are the forces responsible to change the flow pattern throughout the flow path.  $R_{ki}$  represents the friction force from other phases,  $S_{ki}$  is the force due to surface tension from other phases, and  $v_k \Gamma_{ki}$  is the mass transfer or momentum exchange.

### 3.2.2.3 Conservation of Energy

- Considering all the internal and external energy sources acting on the phases, the equation is given as:

$$\begin{aligned} \frac{\delta}{\delta t}(\alpha_k E_k) = & -\frac{\delta}{\delta x}[\alpha_k v_k(E_k + p_k)] + q_{ki} + q_{kw} + w_{ki} \\ & + w_{kw} + \Gamma_{ki}h_{ki} + \Gamma_{kw}h_{kw} \end{aligned} \quad (3.5)$$

The first term represents the internal energy,  $q$  is the specific heat,  $w$  is the specific work,  $\Gamma$  is the specific mass flow term, and  $h$  refers to the specific enthalpy. The subscript “i” and “w” refers to the energy coming from other phases and from outside to a phase  $k$  respectively.

### 3.2.3 $k$ - $\varepsilon$ Turbulence Model

A Computational Fluid Dynamics (CFD) analysis was performed to test number simulations of flux regimes in multiple flux phases, creating a fluid film around a gas bubble and a cause of a slug creation of the flow. The improved performance of the  $k$ - $\varepsilon$  turbulence model was used for different reasons[6], to promote the measurement of digital simulations; (1) the model was very straightforward in format, in comparison to the other complex turbulent model; (2) a  $k$ - $\varepsilon$  turbulence model was a more general model, enabling a quantitative prediction of turbulent clock flow. Many multiple facet flow research studies have demanded compatibility with  $k$ - $\varepsilon$  turbulence model of the non-slip boundary conditions of solid surfaces and of the wall law in calls near solid surfaces (Yadav et al., 2014; De Schepper, 2008; Mazumder, 2012; Valleyet al., 2007; Cook and Kadri et al., 2011).

The two turbulence layer models were used to calculate the turbulent viscosity. The whole computer area divided into a totally turbulent area was represented by a distance near the turbulent Wall of the Reynolds in Eq. (3.6) a viscosity region.

$$\text{Re}_\eta = \frac{\rho\sqrt{k\eta}}{\mu} \quad (3.6)$$

$\eta$  is the normal cell center distance from the wall.

For a low Reynolds number,  $\text{Re}_\eta < 200$ , the low Reynolds number  $k$ - $\varepsilon$  model that was modified by Riverin et al. (2006) was used. Within FLUENT 16.1, the Jones and Laimder model of RNG  $k$ - $\varepsilon$  1972, was improved [18] which significantly improved the accuracy of the turbulent model. This model has been used to avoid the wall functions with the prevailing viscous force for the low Reynolds.

The regulative equations of  $k$  and its dissipation rate  $\varepsilon$  of turbulent fine energy are defined as:

$$\begin{aligned} \frac{\partial(\rho U k)}{\partial x} + \frac{\partial(\rho v k)}{\partial y} = \frac{\partial}{\partial x} \left( \mu + \frac{\mu_T}{\sigma_k} \right) \frac{\partial k}{\partial x} + \frac{\partial}{\partial y} \left( \mu + \frac{\mu_T}{\sigma_k} \right) \frac{\partial k}{\partial y} \\ + \mu_T G' - \rho \varepsilon - 2\mu \left( \frac{\partial k^{1/2}}{\partial y} \right)^2 \end{aligned} \quad (3.7)$$

$$\begin{aligned} \frac{\partial(\rho U \varepsilon)}{\partial x} + \frac{\partial(\rho v \varepsilon)}{\partial y} = \frac{\partial}{\partial x} \left[ \left( \mu + \frac{\mu_T}{\sigma_\varepsilon} \right) \frac{\partial \varepsilon}{\partial x} \right] + \frac{\varepsilon}{k} C_1 f_1 \mu_T G' - \frac{\varepsilon^2}{k} C_2 f_2 \mu_T \rho \\ + 2 \frac{\mu \mu_T}{\rho} \left( \frac{\partial^2 U}{\partial y^2} \right)^2 + \frac{\partial}{\partial y} \left[ \left( \mu + \frac{\mu_T}{\sigma_\varepsilon} \right) \frac{\partial \varepsilon}{\partial y} \right] \end{aligned} \quad (3.8)$$

$k$  and  $\varepsilon$  is combined with the governing equations and the eddy viscosity relationship is known as  $\mu_T = \rho C_\mu k^2 / \varepsilon$ .

### 3.3 Development of Fluid Domain Model

The fluid model is essentially the hollow inner part of the pipe bend model. Three cases of two-phase flow were studied, one using water & air and another using crude oil & natural gas. The flow in the pipeline is the

combination of horizontal and vertical pipeline and is initialized as stratified flow with initial volume fraction of 0.1 for air. Table 5 lists the parameters of pipeline material which is ASTM Carbon Steel A106 GR B as referred from ASME, Section II, Part D and Table 6 lists the boundary conditions that will be used in the simulation.

Table 3.3.1: Pipeline parameters.

Parameters	Value
Total Length	12 m
Pipe Diameter	80 mm
Bending Radius	120 mm
Density	$7.8334 \times 10^{-6}$ kg/mm <sup>2</sup>
Young's Modulus	$1.6608 \times 10^5$ Mpa
Poisson's Ratio	0.3
Bulk Modulus	$1.384 \times 10^5$ Mpa
Shear Modulus	63877 Mpa
Tensile Strength	414 Mpa
Yield Strength	241 Mpa

Table 3.3.2: Boundary Conditions

Boundary Conditions	Remarks
Pipe Pressure	Given along the whole pipe: 2.535 MPa
Standard Earth Gravity:	$9.81 \text{ m/s}^2$ being set downwards, - to Z axis. (- to X axis in ANSYS)
Pipe Temperature: Given along the whole pipe	Referred to ISO DWG stating operating temp at 60°C
Pipe Idealization	As input to software that pipe elbows are to be considered
Horizontal Force	All horizontal sections of pipe, including 45° angled section: 569.37 N
Vertical Force	All vertical sections of pipe, including 45° angle section: 569.37 N
Fluid Mass	10860.742 Kg as distributed load along the pipe. Value taken from pipe volume (11.818m <sup>3</sup> ) and density of working fluid (919 kg/m <sup>3</sup> ).



### 3.4 Meshing of Pipe and Fluid Domain

The meshing of the pipe (solid domain) and the fluid domain are meshed separately each under ANSYS Transient Structural Module and ANSYS CFX module. Both domains are meshed using sweep method with mixed Quad/Tri elements and “Advanced Sizing Function” turned on at curvature.

Coarser mesh is used as a compromise to limited computational resources and time. Table 3 lists the mesh properties difference between FEA and CFD. The meshes are of good quality with aspect ratio well below the recommended maximum aspect ratio of 18-20 by ANSYS documentation. Figure 11 and Table 7 illustrate the mesh quality of both domains.

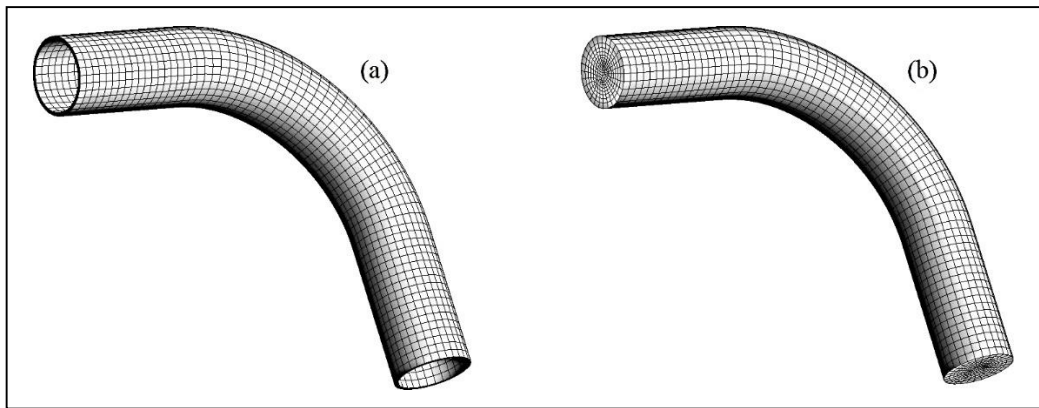


Figure 3.4.1: Mesh Of (A) Pipe Bend (B) Fluid Domain

Table 3.4.1: Difference in Mesh properties of FEA and CFD

Mesh Properties	FEA	CFD
No. of Elements	14122	65678
No. of Nodes	2112	15510
Max Aspect Ratio (<100)	6.22	13.24
Max Skewness (<1)	0.80	0.53

### 3.5 Modal Analysis

Modal analysis is performed in ANSYS Workbench to extract the natural frequencies of the pipe structure under several constraints. Forced vibrations if excited at the same frequency as the natural frequency, resonance will occur and significant vibrations can happen. The natural frequencies and its respective mode shapes are derived according to Eqn. 3.9.

$$[M][\ddot{U}] + [K][U] = 0 \quad (3.9)$$

Where, M is the mass matrix,  $\ddot{U}$  is the acceleration and K is the stiffness matrix.

### 3.6 Screening Methodology

A modal analysis is first performed to extract the natural frequencies of the pipe bend models for each of Case 1 and Case 2 using the Modal Analysis module available in ANSYS Workbench.

Subsequently, the FSI simulations are performed to determine the flow-induced vibration levels and are compared to the natural frequencies extracted. Three locations of interests in the bend are monitored in the simulations (Fig 12).

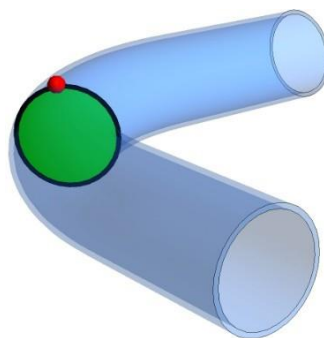


Figure 3.6.1: Locations monitored (At bend)

The first stage of screening is by using the fluctuations in volume fractions of liquid in the fluid domain cross-section plane at the bend (colored in green). The results are then verified with the FSI results in the solid

domain's locations of interests, namely the point colored in red (monitors displacement) and the cross-section plane colored in black (monitors Von Mises Stress) as shown in Table 8. The screening method is in accordance to the screening methodology proposed by Chica (2014).

Table 3.6.1: Properties measured at locations of interest

Location	Properties monitored
Plane in Green	Volume Fraction of Liquid
Plane in Black	Von Mises Stress of Pipe
Red Dot	Displacement of Pipe

### 3.7 Project Process Flow Chart

The project is conducted methodically based on the project process flow chart as shown in Figure 13.

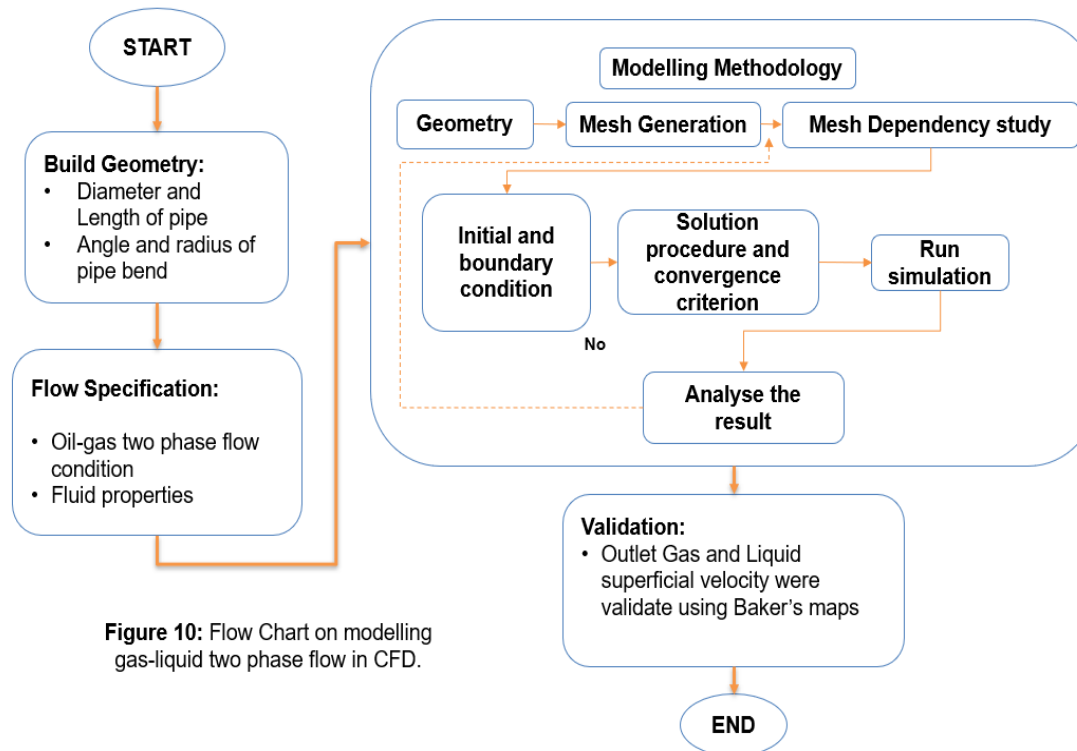


Figure 10: Flow Chart on modelling gas-liquid two phase flow in CFD.

Figure 3.7.1: Project Flow Chart

### 3.8 Project Gantt Chart

Table 3.8.1: Project Gantt Chart

Week number Progress	FYP 1														FYP II													
	1	2	3	4	5	6	7	8	9	10	11	12	13	14	1	2	3	4	5	6	7	8	9	10	11	12	13	14
Background study / Lit. survey			█	█	█	█	█	█	█	█	█	█	█	█														
Identify problem statement, project objectives & scopes of study			█	█		●																						
Familiarization of ANSYS software					█	█	█	█	█	█	█	█	█															
Development of pipe and fluid model									●																			
Simulation model development										█	█	█	█	█	█	█	█	█	█	█	█	█	█	█	█	█	█	
Generate slug flow in pipe using CFD												●	█	█														
Collection of data													█	█														
Modelling of geometry													█	█	●	█												
Result gathering and analysis																█	█	█	█	█	█	●						
Validation of simulation result with Baker's map																				█	█	█	█	█	●			
Project conclusion																							█	█	█	█	█	

● : Key Milestone

CHAPTER 4:  
**RESULTS AND DISCUSSION**

4.1 **Validation of flow pattern on Baker’s map**

Table 4.1.1: Simulation of the air-water operating condition for slug development.

	$G/\lambda$ ( $\text{kgm}^{-2}\text{s}^{-1}$ )	$G$ ( $\text{kgm}^{-2}\text{s}^{-1}$ )	$L \lambda \psi/G$	$L$ ( $\text{kgm}^{-2}\text{s}^{-1}$ )
Slug	3	3	200	600

There is 5 flow pattern that was associated which are stratified flow pattern, wavy flow pattern, slug flow pattern, annular flow pattern and bubble flow pattern. However, this research focused on the slug development in pipeline and its effects on pipe bend. The present simulation was observed and compared with the previous result by De Schepper et al. (2008) and also experimental result by Mohmmmed (2016). The simulation conducted on the geometry of 8m horizontal long tube with 0.08m internal diameter by using the VOF method.

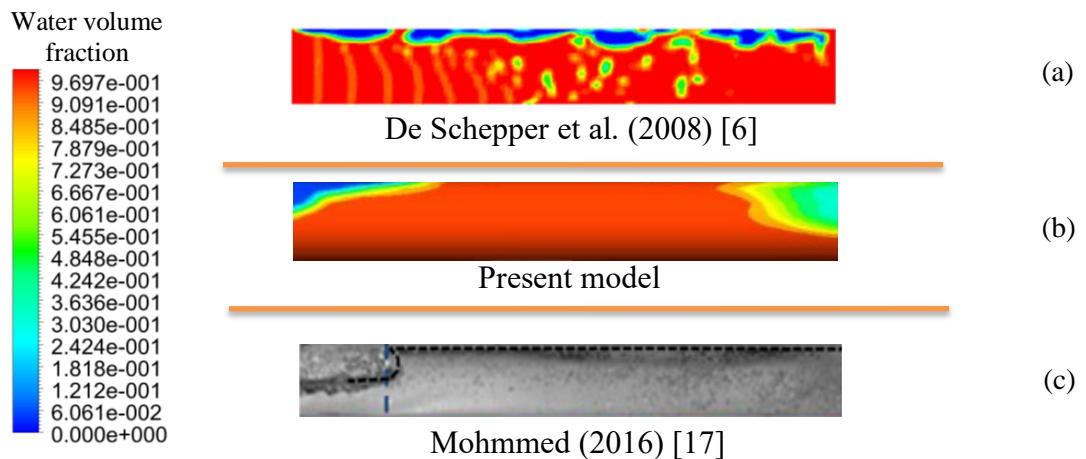


Figure 4.1.1: Contour of water volume fraction on slug development. (a) De Schepper et al. (2008) model, (b) Present model, (c) Mohmmmed (2016) model.

From Figure 4.1.1, (a) De Schepper et al. (2008) shows water volume fraction of the slug-flow pattern. The slug flow pattern can be seen as much more unpredictable compared to the present slug flow system (Figure 4.1.1(b)). However, it must be noted that the liquid slugs do not actually reach the upper part of the tube as

predicted from the Figure 4.1.1(c) observation. Note that the slug flow system is an intermittent flow system, and the slug flow area is located in the center of the Baker map (Figure 2.3.2). As described earlier, large transition zones can be present between the different flow regimes. Because of these transition areas, the area corresponding to the slug flow pattern for water – air flow may be very small relative to the other flow pattern regions, which may explain the simulation results, especially the difficulty of De Schepper et al. (2008) simulating a perfect slug flow regime.

The experimental results are shown in slug flow from Figure 4.1.1 (c). For this form of flow pattern also called intermittent flow where it occurs when the gas velocity is the small and modest liquid velocity. Slug flow formation is due to interface friction between water and air. The motion of the air mixture can come from the flow of turbulence, or from the flow of stratified-wavy pattern. The bubbles will migrate upward to the top of the pipe due to the buoyancy forces, and the extended bubble will shape. The slug flow regime model proves the result of De Schepper et al. (2008) and Mohammed (2016) from the current results obtained.

#### **4.2 The transition of slug flow pattern in a horizontal pipe**

In the current situation, to identify the presence of slug flow are difficult because of the properties of slug and its related criteria such as velocity, the formation of slug and frequency. Figure 4.2 presented the formation of a slug at superficial velocity,  $U_{SG} = 3.07$  m/s and liquid superficial velocity  $U_{SL} = 0.4$  m/s as in inlet boundary condition. Along the pipe, the elongated bubble form is different in length were some with small bubble gas throughout the pipe. The air bubble penetrates more at slug front.

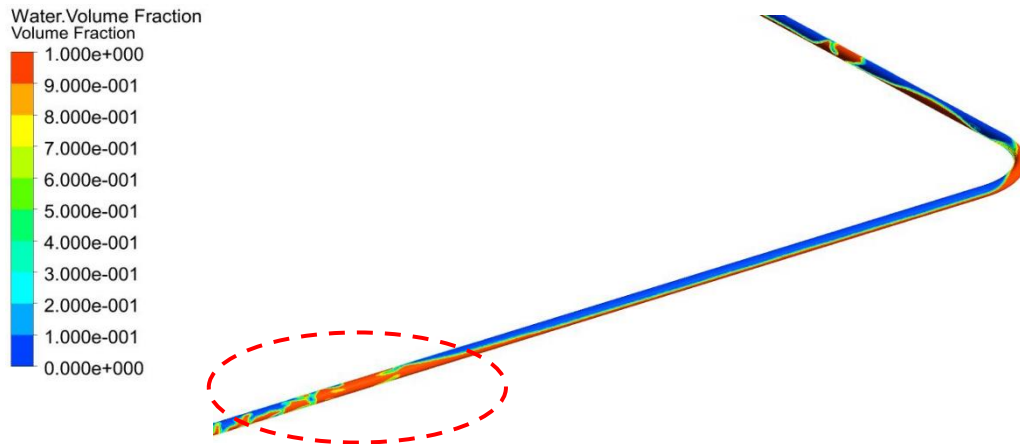


Figure 4.2.1: Water volume fraction contours of slug flow in the pipe.

The colour contour of red signifies liquid while blue refers to gas. The direction flow for this figure is from left the inlet to the right towards the bend before the outlet. The slug flow in the pipe can be clearly observe based on time evolution. The red contour of liquid slug moving to the upper part of the horizontal pipe.

As of Figure 4.2.2, primarily the pipe was filled with an equal volume of air and water with nil velocity. The mixture takes some time in simulation to ensure the formation of the slug to occur as the first crest was formed. The formation of slug starts to grow at time 0.5 second and then continue growing more along the pipe. The short slug was observed from the contour at 1.0 second to 1.5 seconds. This turbulence was taken from the current model and the formation of flow pattern can be observed when the slug passes through the orifice plate geometry of 0.5 diameter ratio.



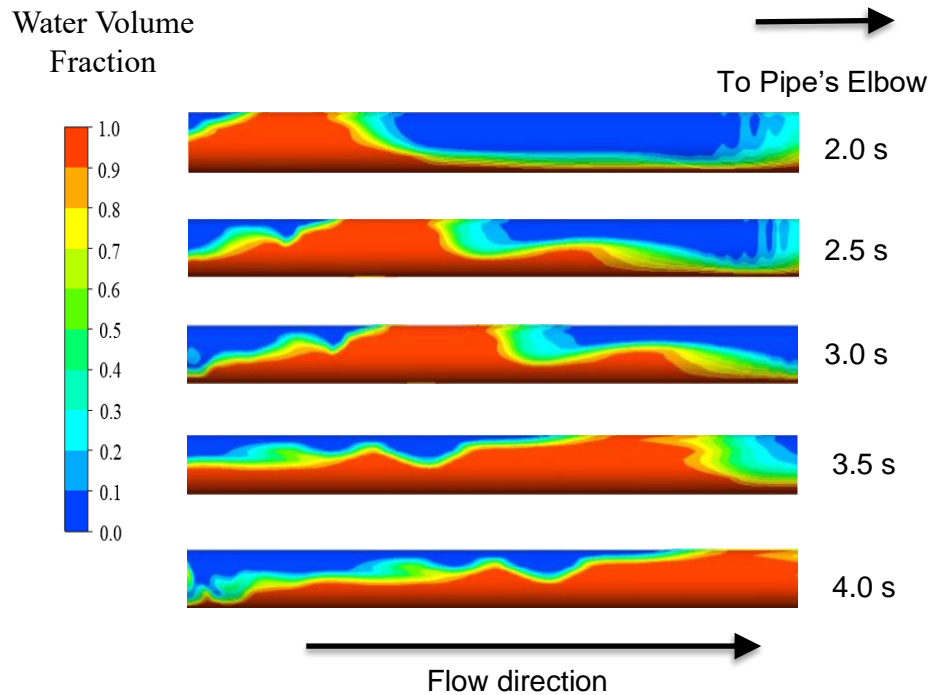


Figure 4.2.2: Time evolution contours of Slug flow and the water volume fraction air-water towards the pipe's elbow for ( $U_{sa} = 3.07$  m/s and  $U_{sw} = 0.4$  m/s).

#### 4.3 Validation of model against Experimental figures

For this parts, the present model of CFD model simulation was used to compare with the experimental result as for validation to guarantee the rightness and assurance of current work. The prediction of CFD simulation was computed with an experimental photograph.

##### 4.3.1 The Experimental test methodology

For the previous validation of slug flow, it was validated based on the concept. For this experimental test that been done by Dinaryanto et al. (2017) [16], it will be used to compare with a present simulation model. The geometry of experimental test was executed at 0.026 m of internal diameter and length of 10 m. Type of fluid used for this type of experiment is air-water which are two-phase flow. The atmospheric pressure, 101.3 kPa and room temperature, 24°C are been used respectively. From Figure 4.3.1 illustrate the schematic diagram of the experimental apparatus.

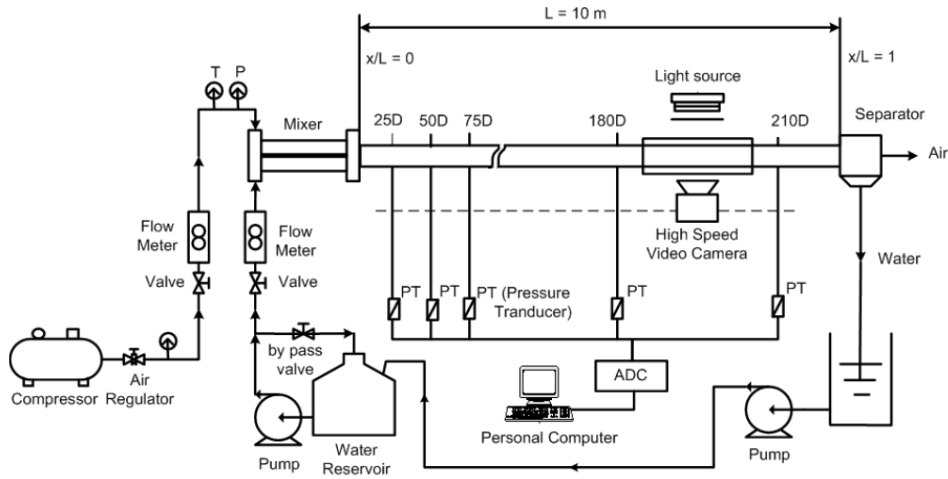


Figure 4.3.1: The schematic diagram of the experimental apparatus [16].

### 4.3.2 CFD of slug development comparison between Experiment photographs.

The following stage of slug formation between the current model simulation and experimental snapshots are shown in Figure 4.3.2. Initially, the water volume fraction of liquid and air are 50% as shown in Figure 4.3.2 (a) as the slug starts to initiate. As been shown in Figure 4.3.2 (b) and (c), the red contour of water volume fraction shows small crest develop the liquid hold up increase in form of slug liquid  $H_{Ls} = 0.55$ . When the superficial velocity of the liquid set to 0.77 m/s, the thrust of the liquid increase rapidly which causes the slug flow pattern to form and advanced along the pipe.

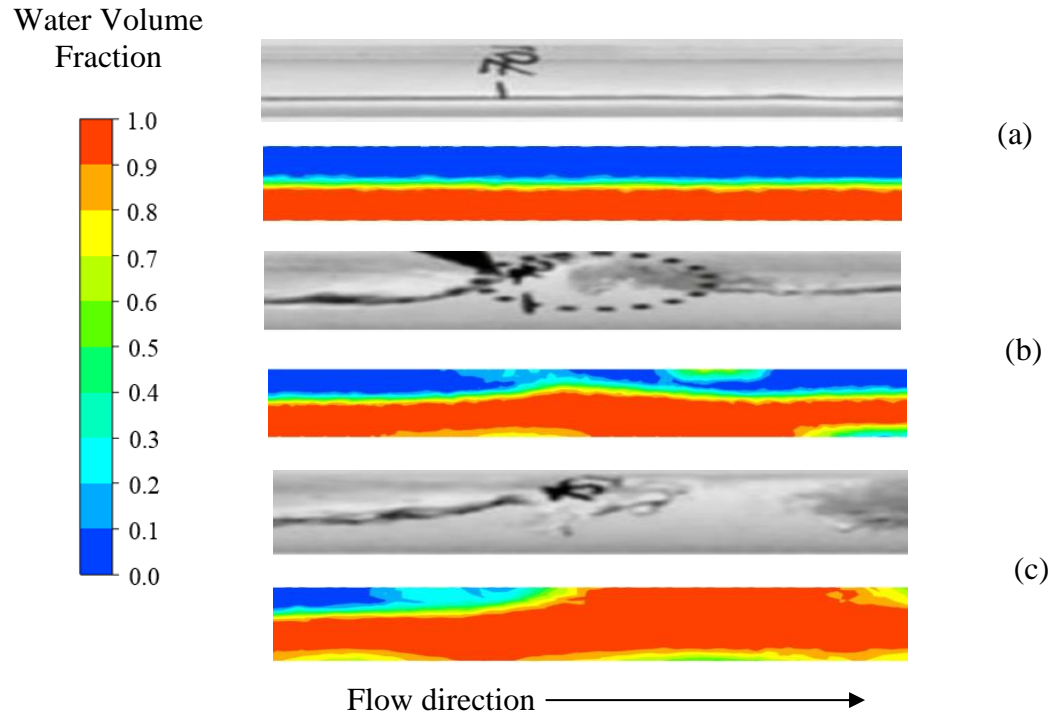


Figure 4.3.2: The evaluation of slug progression between experimental work and CFD data simulation on water volume fraction for  $U_{sa} = 1.88$  m/s,  $U_{sw} = 0.77$  m/s (a) Stratified pattern, (b) Crest jump and (c) slug pattern.

The assessment of slug flow pattern throughout the horizontal pipeline was recorded between current work model from CFD simulation and experimental has been presented in Figure 4.3.3. The inlet boundary condition for the slug in the pipe are at  $U_{SG} = 1.88$  m/s and  $U_{SL} = 0.77$  m/s. From the experimental photographs and water volume fraction, contour has been illustrated shows a strong and reasonable comparison. The volume of fluid (VOF) method was used to obtain the water and air boundary.

Figure 4.3.3 shows the slug flow region start to appear. According to the experimental methodology, the picture of the slug flow pattern was taken based on camera resolution of 1920 x 1080 with 1.20 m length. For Figure 4.3.3 the actual length of 1-centimetre scale signified 0.034 meters. Thus, from the first picture taken shows that the total slug length is 0.105 m as shown in Figure 4.3.3.

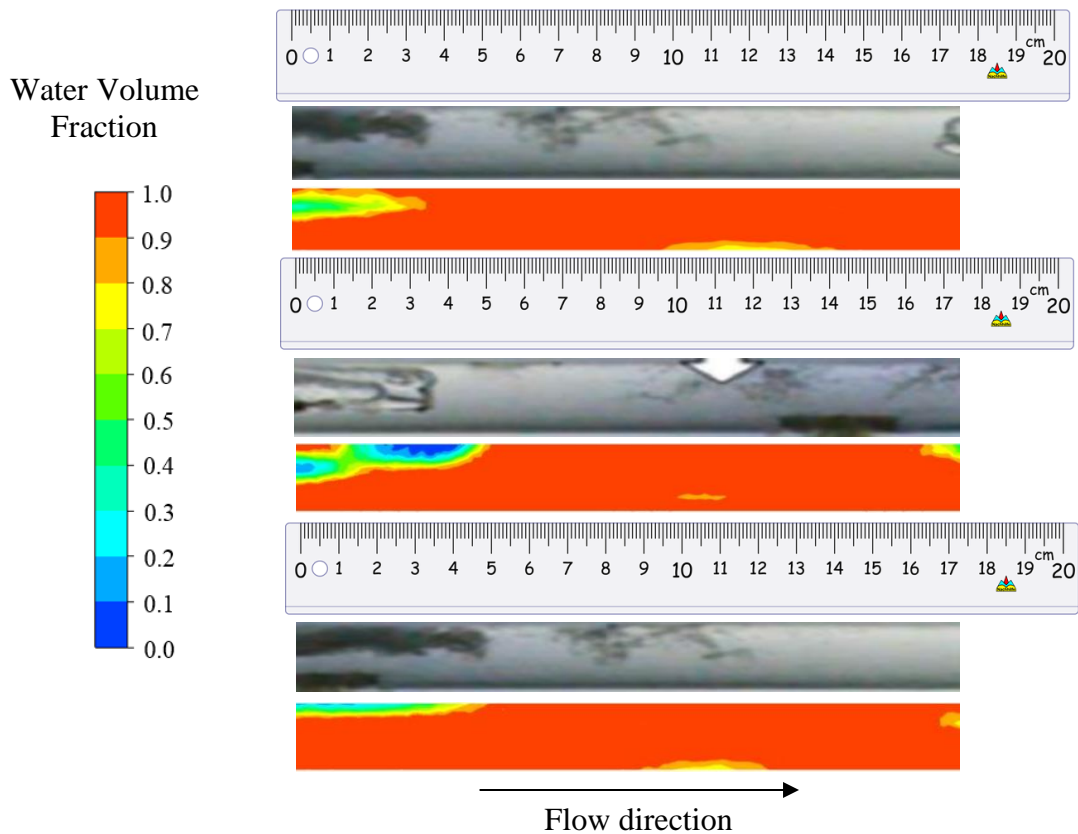


Figure 4.3.3: Contour of Slug flow water volume fraction, snapshot of experimental works and simulation for  $U_{sa} = 1.88$  m/s,  $U_{sw} = 0.77$  m/s.

#### 4.4 Parametric analysis on diameter ratio of the orifice plate

The parametric analysis was studied and directed for different air superficial velocity in a horizontal pipeline. The length of total of the horizontal pipe was set to be 8 m. The main diameter for the horizontal pipe was 0.08 m in diameter. There are three different air superficial velocity which are 3.08 m/s, 4.77 m/s and 6.45 m/s. The water inlet superficial velocity was set to be constant at 0.4 m/s for the whole simulations. Table 4.4.1.

Table 4.4.1: The inlet boundary condition for parametric study.

Bending radius over diameter of pipe, r/D	Air inlet superficial velocity, m/s	Water inlet superficial velocity, m/s
1	3.08	0.4
	4.77	
	6.45	
1.5	3.08	
	4.77	
	6.45	
3	3.08	
	4.77	
	6.45	

#### 4.4.1 Parametric analysis of air inlet superficial velocity on slug development.

Since the volume of one phase cannot be substituted for the other phases, the concept of the volume fraction is implemented. Such volume fractions are called continuous space functions and are equivalent to one number. For each point, conservation equations are derived in order to obtain a set of equations with similar structures for all stages in order to validate the superficial velocity principle.

Water Volume Fraction vs Flow-time

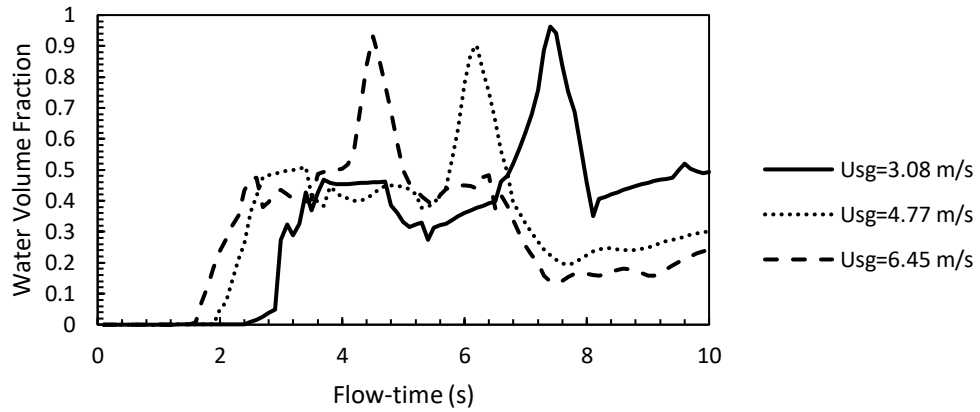


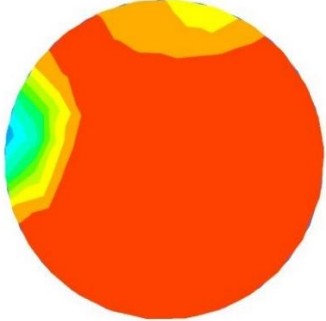
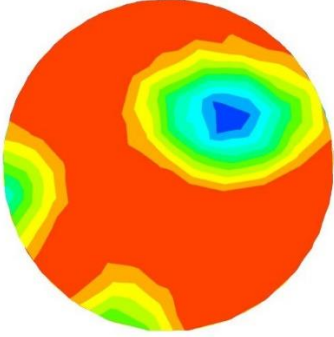
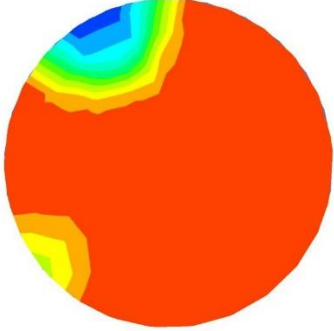
Figure 4.4.1: Time record of water volume fraction on the cross sectional pipe located before elbow when increases air superficial velocity from 3.08 m/s to 6.45 m/s with constant water superficial velocity,  $U_{sw} = 0.4$  m/s.

Table 4.4.2 shows the approximate time for slug to arrive at pipe’s elbow. When superficial air velocity increased from 3.08 m/s to 6.45 m/s, the slug development become faster. The contour of water volume fraction was tabulated in Table 4.4.3.

Table 4.4.2: Approximate time for Slug to arrive at pipe’s elbow.

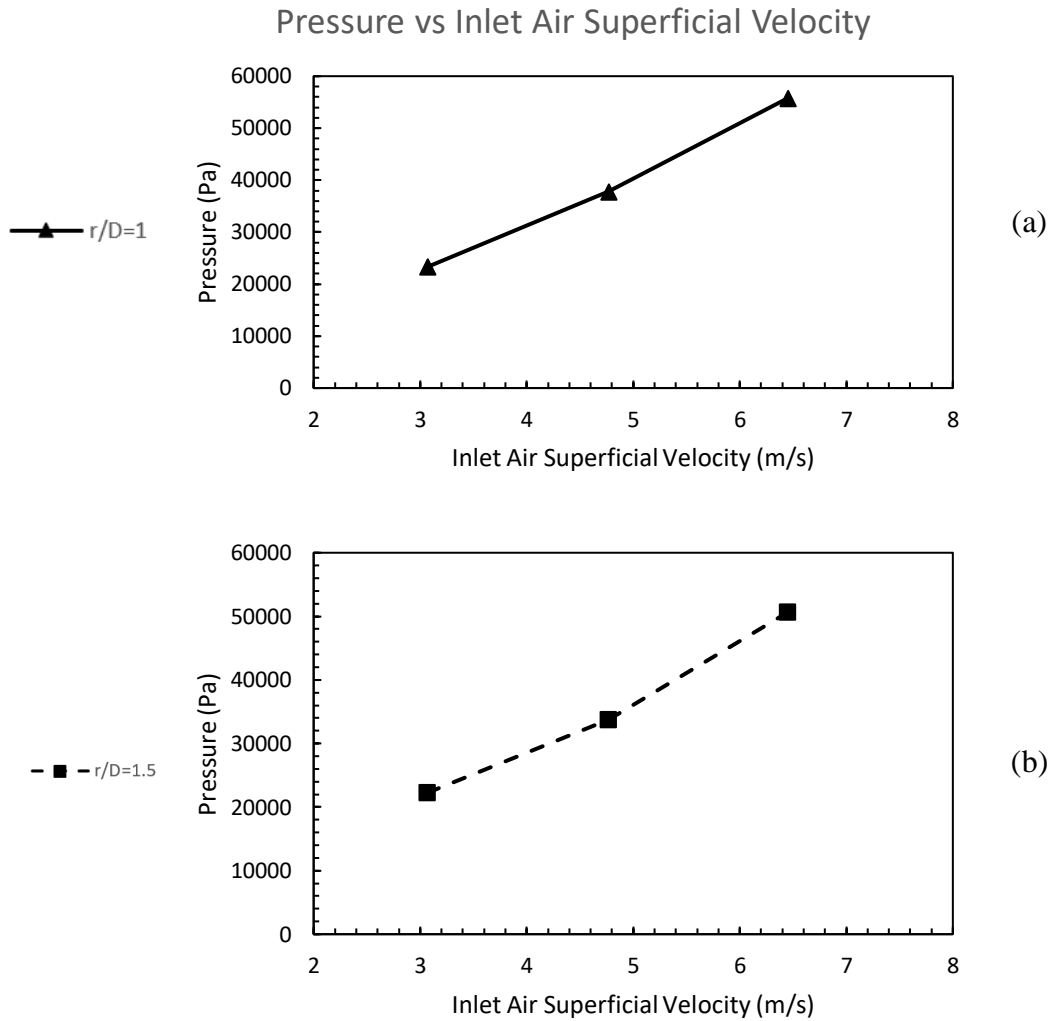
Air inlet Superficial Velocity (m/s)	3.08	4.77	6.45
Time to form Slug (s)	7.4	6.2	4.5
Max Volume Fraction (-)	0.962	0.902	0.931

Table 4.4.3: Water volume fraction contour on slug development for each condition of air inlet superficial velocity

Air Superficial Velocity (m/s)	Water Volume Fraction (-)
3.08	
	0.962
4.77	
	0.902
6.45	
	0.931

#### 4.4.2 Parametric analysis of air inlet superficial velocity towards exerted pressure on the wall of the elbow.

According to Baker's flow regime maps, there are specific ranges of inlet air and water superficial velocity of a pipeline for various pattern of flow regimes. This research focused on the study of slug flow pattern and its effects towards the elbow of pipeline. Figure 4.4.2.





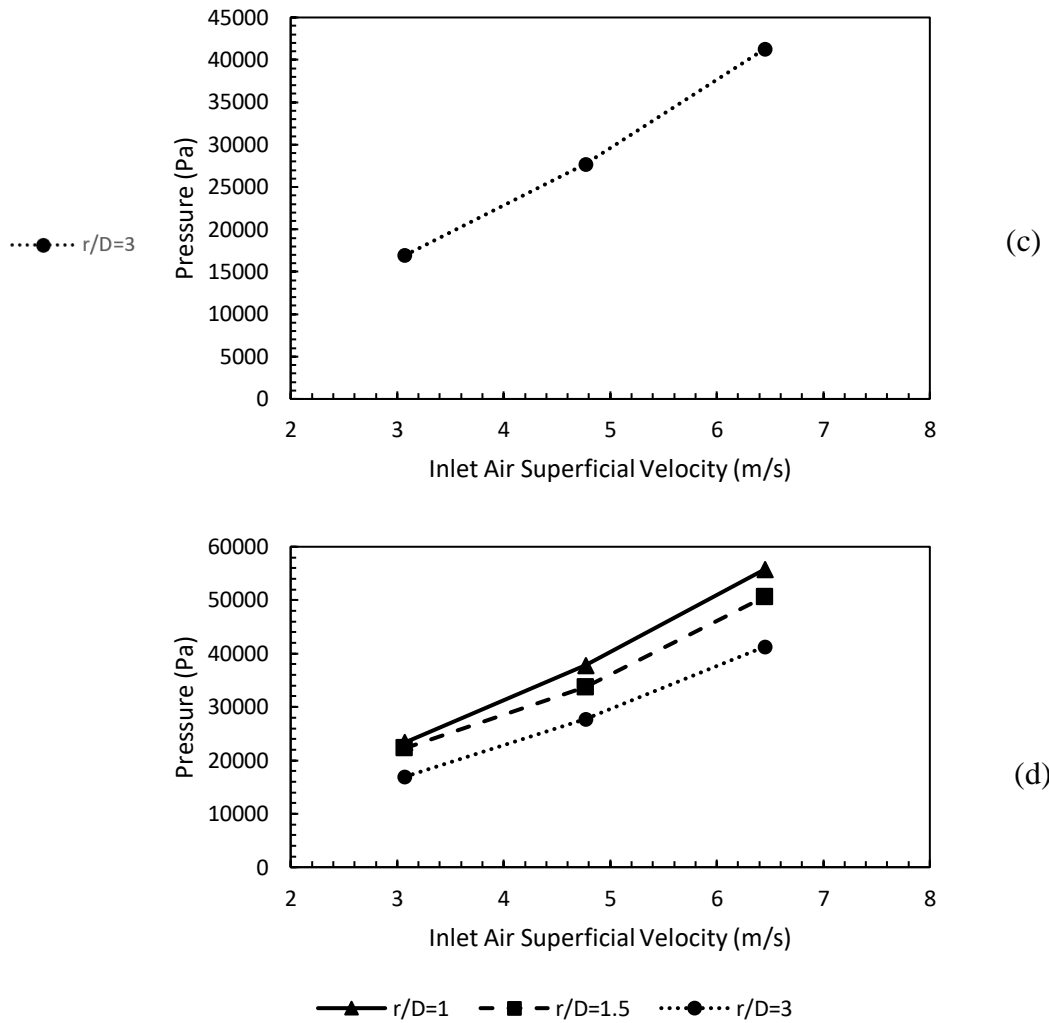
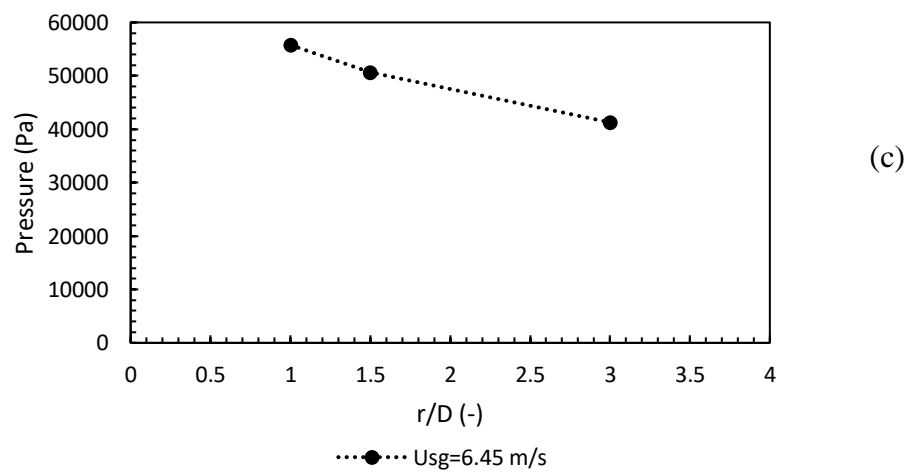
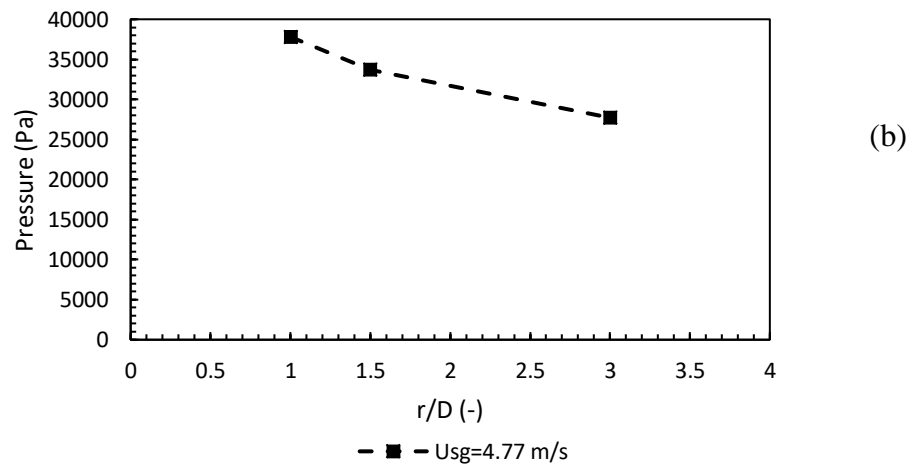
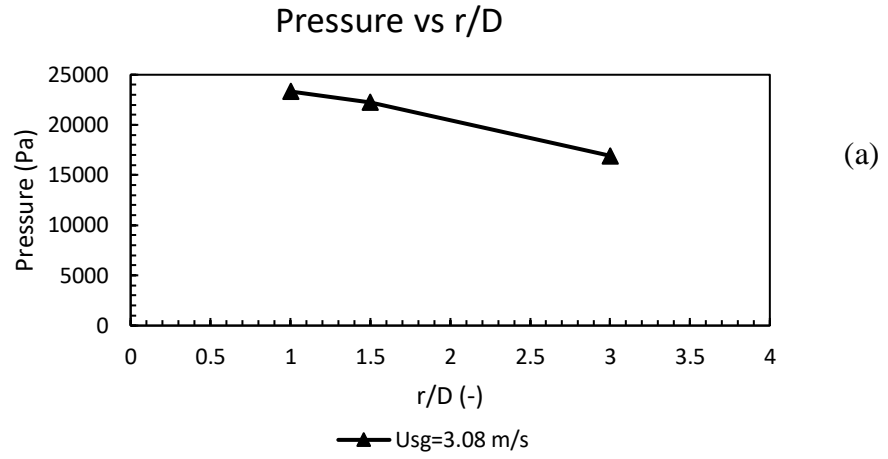


Figure 4.4.2: The total exerted pressure on elbow's wall against air inlet superficial velocity with  $r/D$  ratio from 1.0 to 3.0 for graph (a) (b) (c) (d) with constant inlet  $U_{sw} = 0.4$  m/s.

Figure 4.4.2 above shows the graph of total pressure against the air inlet superficial velocity for slug flow that passes through the  $90^\circ$  elbow of the pipe with varies bending radius over pipe diameter ratio of 1.0, 1.5 and 3.0. The point data were plot by making inlet superficial velocity of the air as manipulating variable from 3.08 m/s to 6.45 m/s whereas water inlet superficial velocity as a constant variable for case (a) (b) (c) and (d) which is  $U_{SL} = 0.4$  m/s. The result concludes that the higher the air inlet superficial velocity will produce a higher total pressure exerted on the inner part of pipe elbow.

Further study on the parameter analysis of pipe bending radius over pipe diameter ratio,  $r/D$  has been done in this research to analyse the effect of  $r/D$  ratio to the total

pressure exerted on the inner part of pipe elbow. Figure shows the relations on the parameter studied for this analysis.



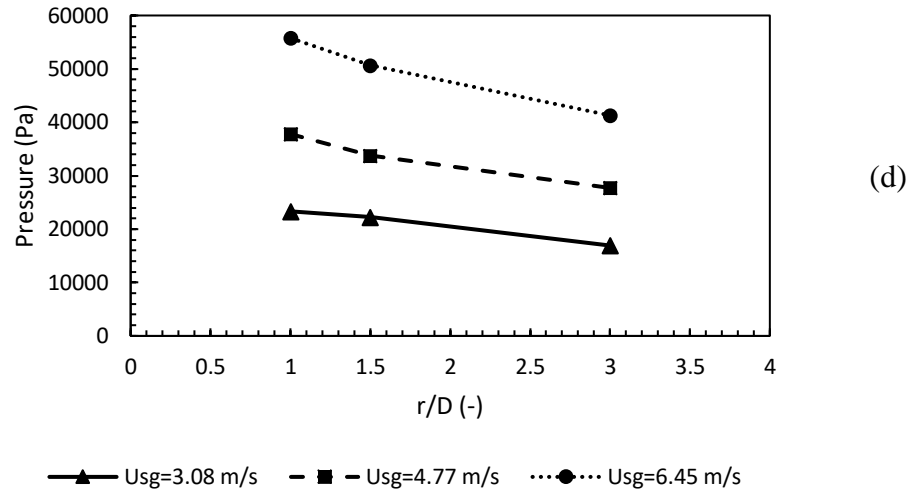
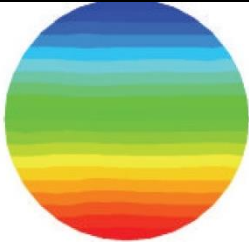
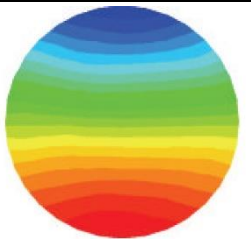
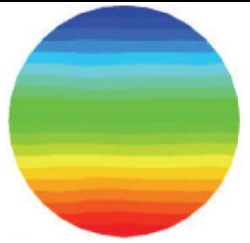
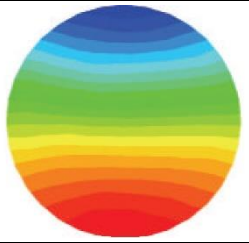
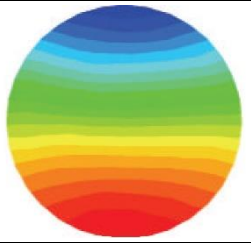
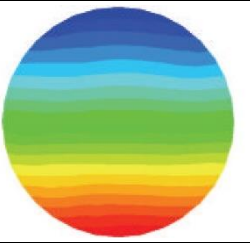
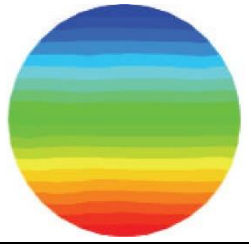
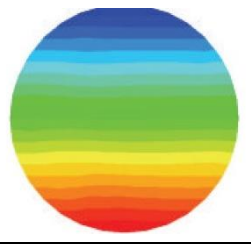
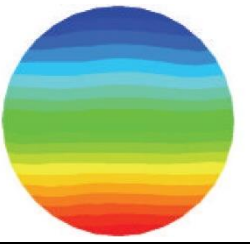
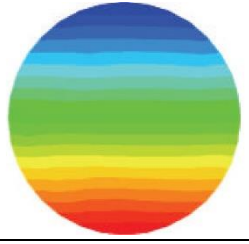
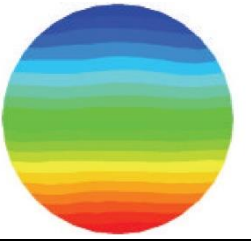
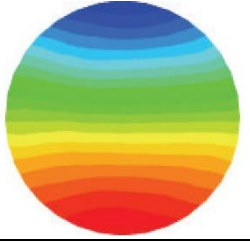
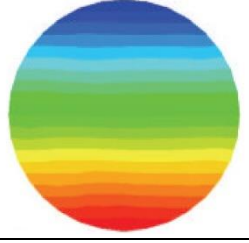
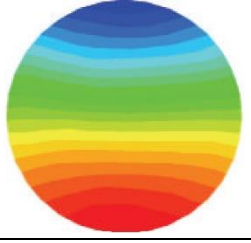
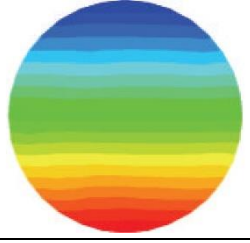


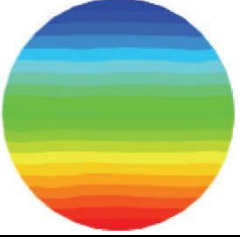
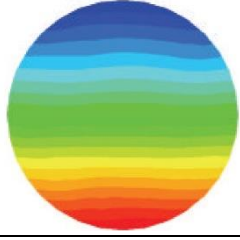
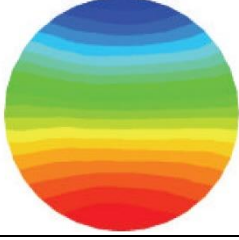
Figure 4.4.3: The total exerted pressure on elbow's wall against  $r/D$  ratio with air inlet superficial velocity from 3.07 m/s to 6.45 m/s for graph (a) (b) (c) (d) with constant inlet  $U_{sw} = 0.4$  m/s.

Table 4.4.4 displays the absolute pressure contour on two specific locations on the pipe which are located at the beginning and the end of the pipe elbow which was defined as Measurement Section 1 and Measurement Section 2 (refer to pipe geometry model). The result concludes that the higher the air inlet superficial velocity will produce a higher pressure drop across the pipe elbow. However, a significant higher-pressure drop can be observed based on the result when decreasing the bending radius over pipe diameter ratio,  $r/D$ .

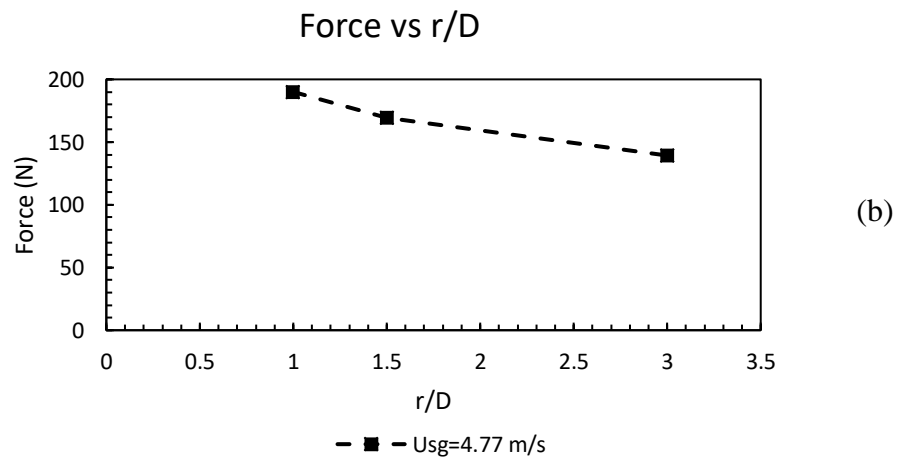
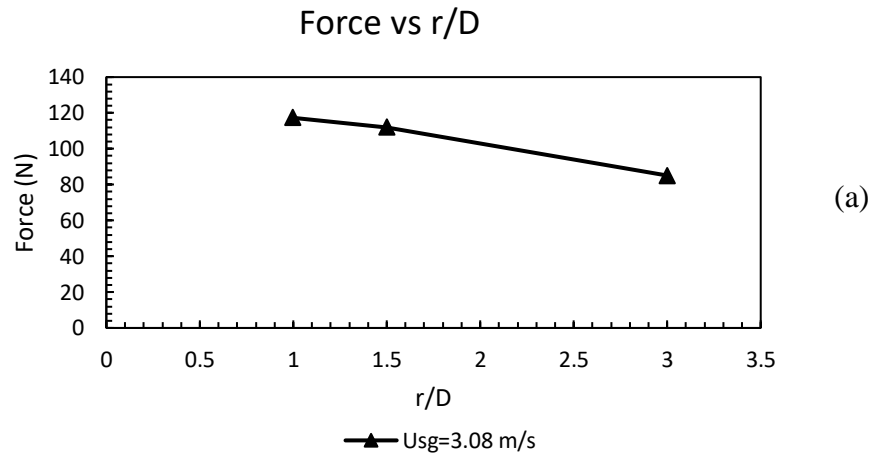
Table 4.4.4: Pressure Contour at Measurement Section 1 and 2 with varies value of  $r/D$  ratio and air superficial velocity at constant inlet  $U_{sw} = 0.4$  m/s.

Absolute Pressure Contour				
Location	r/D	Air: 3.08 m/s	Air: 4.77 m/s	Air: 6.45 m/s
Measurement Section 1	1.0			
		$P_{\max} = 191.63$ kPa	$P_{\max} = 193.31$ kPa	$P_{\max} = 195.28$ kPa
	1.5			
		$P_{\max} = 191.27$ kPa	$P_{\max} = 194.74$ kPa	$P_{\max} = 195.93$ kPa
	3.0			
		$P_{\max} = 191.82$ kPa	$P_{\max} = 193.21$ kPa	$P_{\max} = 196.17$ kPa

Absolute Pressure Contour				
Location	r/D	Air: 3.08 m/s	Air: 4.77 m/s	Air: 6.45 m/s
Measurement Section 2	1.0			
		$P_{\max} = 185.94$ kPa	$P_{\max} = 187.27$ kPa	$P_{\max} = 190.39$ kPa
	1.5			
		$P_{\max} = 188.45$ kPa	$P_{\max} = 190.83$ kPa	$P_{\max} = 192.72$ kPa

	3.0			
		$P_{\max} = 189.87 \text{ kPa}$	$P_{\max} = 192.52 \text{ kPa}$	$P_{\max} = 194.34 \text{ kPa}$

#### 4.4.3 Parametric analysis of air inlet superficial velocity and r/D ratio on resultant force exerted on the inner part of pipe elbow.



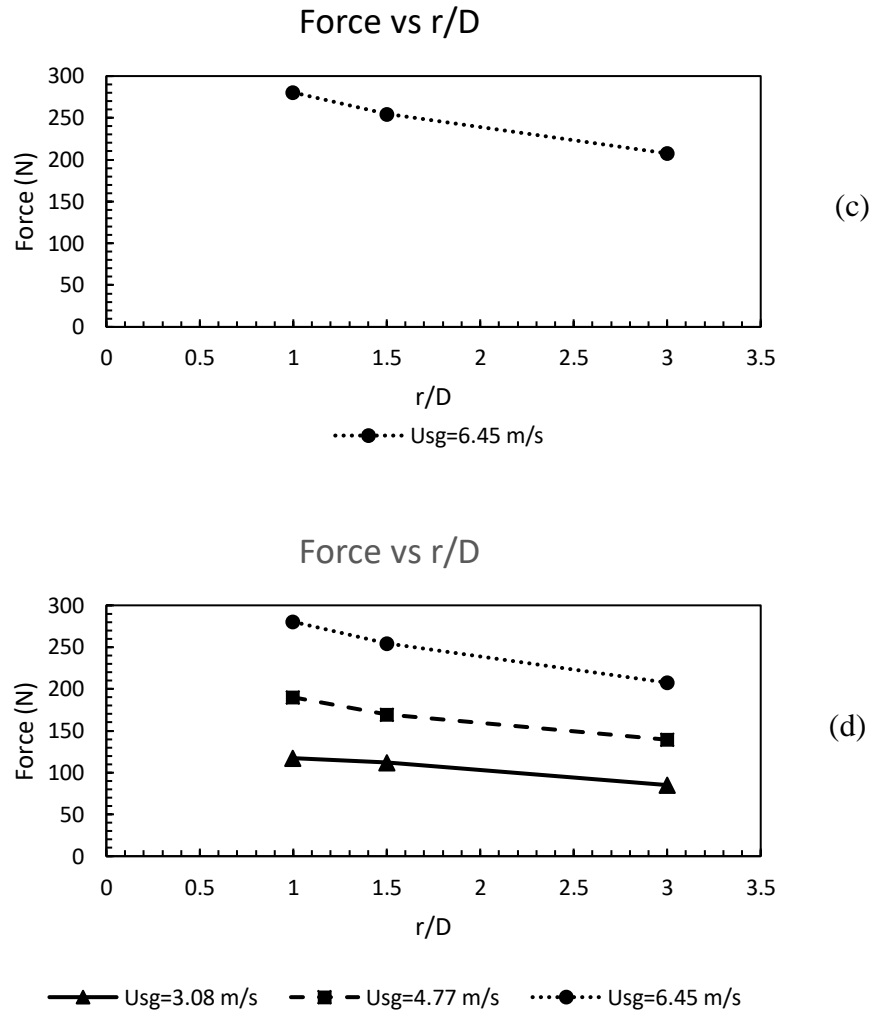


Figure 4.4.4: The resultant force on elbow's wall against r/D ratio with air inlet superficial velocity from 3.08 m/s to 6.45 m/s for graph (a) (b) (c) (d) with constant inlet  $U_{sw} = 0.4$  m/s.

Based on Figure 4.10 shows the graph of resultant force on the inner part of pipe elbow against the bending radius over pipe diameter ratio, r/D for slug flow that passes through the 90° pipe elbow with a r/D ratio of 1.0, 1.5 and 3.0. The point data were plotted by making inlet superficial velocity of the air as manipulating variable from 3.08 m/s to 6.45 m/s whereas water inlet superficial velocity as a constant variable for case (a) (b) (c) and (d)  $U_{SL} = 0.4$  m/s. The result concludes that the higher the bending radius over pipe diameter ratio, r/D will produce a lower resultant force exerted on the inner part of pipe elbow while higher air inlet superficial velocity results in lower resultant force acted on the inner part on the pipe elbow.

## CHAPTER 5:

### CONCLUSIONS AND RECOMMENDATIONS

Pipelines work as a transport medium in transporting medium among or more remote stations. Fluid flow pattern inside horizontal pipes consists of gas and liquid happened in the production of fuel and gas industry. Piping is the common medium for these types of industry to transport the liquid. Horizontal bending pipe geometry has been selected as a research parameter to correlate the bending radius over pipe diameter ratio,  $r/D$  to the resulting level of flow induced vibration arising from slug flow in the pipe. For these researches, volume of fluid (VOF) method was used where it is the model that is able to produce excellent surface result simulation for slug flow. Air and water were selected as an operating condition for these projects in the horizontal pipe.

The validation result of the present model of flow regime is equivalent to the research paper from De Schepper [6] that refer to the Baker's flow regime map. The simulation was done for the present model use the VOF method. Moreover, the present work obtained a similar slug flow pattern in the horizontal pipe. The research then covers the  $r/D$  ratio with different  $r/D$  values in a horizontal bending pipeline. In addition, the slug development become faster when superficial velocity increased from 3.08 m/s to 6.45 m/s as possibly due to the increase of likely turbulence flow in the pipe. The slug that was developed in the pipe was indicated by the reading of the flow water volume fraction which was equally to the value of nearest to 1.

It can be concluded that the pressure exerted on the inner part of pipe elbow increases when the inlet superficial velocity of air increases while the higher the value of  $r/D$  of a pipe will results in a lower pressure exerted on the inner part of an elbow. Due to the sudden change of the direction of the flow, the slug that was developed in the pipe produces a high-pressure impact on the inner part of the pipe elbow which was also interpreted as the high resultant force exerted on the inner part of the elbow's wall. This high resultant force will then be causing a vibration phenomenon on the wall of the pipe and the main cause for this vibration is highly related to the differential pressure (pressure loss) which occurs across the elbow of the pipe.

As part of the recommendation, future works for improvement that could be done in the future are by furthering the research to three-phase flow that considered oil, gas, and water in the simulation. The studies will be similar to the baker's map flow regime. Other than that, use a vertical bending pipe with various bending angles such as  $45^\circ$ ,  $135^\circ$  and U-shaped pipe bend as the parametric study to observe the effect of pipe bend angle to the resulting level of induced vibration on the pipe. Finally, use more data point to obtain a better trend for the results.



## REFERENCES

- [1] K. Havre, K.O. Stornes and H. Stray. (2000, April). Taming slug flow in pipelines. [Online]. Available: [http://www02.abb.com/global/seitp/seitp161.nsf/viewunid/8A01902E860EAE9185256B57006D9803/\\$file/ABBReview2000.pdf](http://www02.abb.com/global/seitp/seitp161.nsf/viewunid/8A01902E860EAE9185256B57006D9803/$file/ABBReview2000.pdf)
- [2] W. Peng and X. Cao, “Numerical simulation of solid particle erosion in pipe bends for liquid–solid flow,” *Powder Technology*, vol. 294, pp. 266-279, 2016.
- [3] D. H. Kim and S. H. Chang, “Flow-induced vibration in two-phase flow with wire coil inserts” *International Journal of Multiphase Flow*, vol. 34, (4), pp. 325-332, 2008.
- [4] B. L. Tay and R. B. Thorpe, “Effects of liquid physical properties on the forces acting on a pipe bend in gas–liquid slug flow,” *Chemical engineering research and design*, vol. 82, (3), pp. 344-356, 2004
- [5] M. S. Yadav, T. Worosz, S. Kim, K. Tien and S. M. Bajorek, “Characterization of the dissipation of elbow effects in bubbly two-phase flows,” *International Journal of Multiphase Flow*, vol. 66, pp. 101-109, 2014.
- [6] S. C. De Schepper, G. J. Heynderickx and G. B. Marin, “CFD modeling of all gas–liquid and vapor–liquid flow regimes predicted by the Baker chart,” *Chemical Engineering Journal*, vol. 138, (1-3), pp. 349-357, 2008.
- [7] L. Chica, “Fluid Structure Interaction Analysis of Two-Phase Flow in an M-shaped Jumper,” in *Star Global Conference 2012*, University of Houston, Houston, United States, 2012.
- [8] Q.H. Mazumder, “CFD Analysis of the Effect of Elbow Radius on Pressure Drop in Multiphase Flow,” University of Michigan-Flint, USA, 2012.

- [9] C. Vallee, H. Hohne, H.M. Prasser and T. Suhnel, "Experimental Investigation and CFD Simulation of Horizontal Stratified Two-phase Flow Phenomena," *Forschungszentrum Rossendorf e. V.*, Dresden, Germany. 2007.
- [10] Y. Liu, S. Miwa, T. Hibiki, M. Ishii, H. Morita, Y. Kondoh, et al., "Experimental study of internal two-phase flow induced fluctuating force on a 90° elbow," *Chemical Engineering Science*, vol. 76, pp. 173-187, 2012.
- [11] U. Kadri, R. Henkes, R. Mudde, and R. Oliemans, "Effect of gas pulsation on long slugs in horizontal gas-liquid pipe flow," *International journal of multiphase flow*, vol. 37, pp. 1120-1128, 2011.
- [12] J.L. Riverin and M. Pettigrew, "Vibration excitation forces due to two-phase flow in piping elements," *Journal of Pressure Vessel Technology*, vol. 129, pp. 7-13, 2007.
- [13] J. Riverin, E. De Langre, and M. Pettigrew, "Fluctuating forces caused by internal two-phase flow on bends and tees," *Journal of sound and vibration*, vol. 298, pp. 1088-1098, 2006.
- [14] Z. I. Al-Hashimy, H. H. Al-Kayiem, R. W. Time, and Z. K. Kadhim, "Numerical Characterisation of Slug Flow in Horizontal Air/water Pipe Flow," *International Journal of Computational Methods and Experimental Measurements*, vol. 4, pp. 114-130, 2016.
- [15] H. Abdulmouti, "Bubbly two-phase flow: Part I-characteristics, structures, behaviors and flow patterns," *American Journal of Fluid Dynamics*, vol. 4, (4), 194-240. 2014.
- [16] O. Dinaryanto, Y. A. K. Prayitno, A. I. Majid, A. Z. Hudaya, Y. A. Nusirwan, A. Widyaparaga, Indarto and Deendarlianto, "Experimental investigation on the initiation and flow development of gas-liquid slug two-phase flow in a horizontal pipe," *Experimental Thermal and Fluid Science*, vol. 81, pp. 93-108, 2017.

- [17] A. O. Mohmmmed, "Effect of slug two-phase flow on fatigue of pipe material," Ph.D Dissertation, Department of Mechanical Engineering, Universiti Teknologi PETRONAS, Malaysia. 2016
- [18] Z. I. Al-Hashimy, H. H. Al-Kayiem and R. W. Time, "Experimental investigation on the vibration induced by slug flow in horizontal pipe," *ARPJ. Eng. Appl. Sci*, vol. 11, pp. 12134-12139, 2016.
- [19] D. Q. Hou, A. S. Tijsseling, and Z. Bozkus, "Dynamic force on an elbow caused by a traveling liquid slug," *Journal of Pressure Vessel Technology*, vol. 136, (3), 2014.
- [20] S. Miwa, M. Mori and T. Hibiki, "Two-phase flow induced vibration in piping systems," *Progress in Nuclear Energy*, vol. 78, pp. 270-284, 2015.